
Article:
Hedin, J, Giovane, F, Waldemarsson, T et al. (13 more authors) (2014) The MAGIC meteoric smoke particle sampler. Journal of Atmospheric and Solar-Terrestrial Physics, 118 (Part B). 127 - 144. ISSN 1364-6826

https://doi.org/10.1016/j.jastp.2014.03.003

The MAGIC meteoric smoke particle sampler

Jonas Hedin[a*], Frank Giovane[b,c], Tomas Waldemarsson[a,b], Jörg Gumbel[a], Jürgen Blum[d], Rhonda M. Stroud[e], Layne Marlin[b], John Moser[b], David E. Siskind[b], Kjell Jansson[f], Russell W. Saunders[g], Michael E. Summers[h], Philipp Reissaus[i], Jacek Stegman[a], John M. C. Plane[g], Mihály Horányi[j].

[a] Department of Meteorology, Stockholm University (MISU), 10691 Stockholm, Sweden.
[b] Space Science Division, Naval Research Laboratory (NRL), Washington D.C., USA.
[c] Virginia Polytechnic Institute, Physics Department, Blacksburg, VA, USA.
[d] Technical University Braunschweig, Braunschweig, Germany.
[e] Materials Science and Technology Division, Naval Research Laboratory, Washington D.C., USA.
[f] Department of Materials and Environmental Chemistry, Stockholm University, Stockholm, Sweden.
[g] School of Chemistry, University of Leeds, Leeds, U.K.
[h] Georg Mason University, Fairfax, VA, USA.
[i] Space Technologies & Applications Division, Kayser-Threde GmbH München, 81379 München, Germany.
[j] University of Colorado, Boulder, CO, USA.

Corresponding author:
Jonas Hedin, jonash@misu.su.se, tel: +46-8-164232, fax: +46-8-157185
Department of Meteorology, Stockholm University, 10691 Stockholm, Sweden

Manuscript for submission to the special issue
Smoke and Ice in the Mesosphere
in *Journal of Atmospheric and Solar-Terrestrial Physics*
November 2013

Abstract

Between a few tons to several hundred tons of meteoric material enters the Earth's atmosphere each day, and most of this material is ablated and vaporized in the 70 to 120 km altitude region. The subsequent chemical conversion, re-condensation and coagulation of this evaporated material are thought to form nanometre sized meteoric smoke particles (MSPs). These smoke particles are then subject to further coagulation, sedimentation and global transport by the mesospheric circulation. MSPs have been proposed as a key player in the formation and evolution of ice particle layers around the mesopause region, i.e. noctilucent clouds (NLC) and polar mesosphere summer echoes (PMSE). MSPs have also been implicated in mesospheric heterogeneous chemistry to influence the mesospheric odd oxygen/odd hydrogen (O_x/HO_x) chemistry, to play an important role in the mesospheric charge balance, and to be a significant component of stratospheric aerosol and enhance the depletion of O_3.

Despite their apparent importance, little is known about the properties of MSPs and none of the hypotheses can be verified without direct evidence of the existence, altitude and size distribution, shape and elemental composition. The aim of the MAGIC project (Mesospheric Aerosol – Genesis, Interaction and Composition) was to develop an instrument and analysis techniques to sample for the first time MSPs in the mesosphere and return them to the ground for detailed analysis in the laboratory. MAGIC meteoric smoke particle samplers have been flown on several sounding rocket payloads between 2005 and 2011. Several of these flights concerned non-summer mesosphere conditions when pure MSP populations can be expected. Other flights concerned high latitude summer conditions when MSPs are expected to be contained in ice particles in the upper mesosphere. In this paper we present the MAGIC project and describe the MAGIC MSP sampler, the measurement procedure and laboratory analysis. We also present the attempts to retrieve MSPs from these flights, the challenges inherent to the sampling of nanometre sized particles and the subsequent analysis of the sampled material, and thoughts for the future. Despite substantial experimental efforts, the MAGIC project has so far failed to provide conclusive results. While particles with elemental composition similar to what is to be expected from MSPs have been found, the analysis has been compromised by

challenges with different types of contamination and uncertainties in the sticking efficiency of the particles on the sampling surfaces.

1. Introduction

The Earth´s atmosphere is constantly bombarded by meteoric material. The total amount of this incoming material is a subject of controversy (Plane, 2012) with estimates ranging from a few tons to several hundred tons per day (Hughes, 1978; Love and Brownlee, 1993; Ceplecha et al., 1998; Cziczo et al., 2001; Mathews et al., 2001; Gabrielli et al., 2004; Plane, 2004; von Zahn, 2005). Most of this material is expected to vaporise in the altitude region 70 – 120 km during atmospheric entry (e.g. Ceplecha et al., 1998; Vondrak et al., 2008). It is well known that this ablation is the source of the global layers of metal atoms and ions that are observed by ground-based (e.g. Chamberlain et al., 1958; Bowman et al., 1969; Kane and Gardner, 1993; Alpers et al., 1996; Eska et al., 1998; Plane, 2003) and satellite- and rocket-borne (e.g. Donahue and Meier, 1967; Donahue et al., 1972; Newman, 1988; Kopp, 1997; Aikin et al., 2004; Fussen et al., 2010; Hedin and Gumbel, 2011) instruments in the mesosphere and lower thermosphere (MLT) region. Chemical conversion and subsequent re-condensation and coagulation of the vaporised material is thought to give rise to tiny nanometre size meteoric smoke particles, MSPs, which are then subject to further coagulation, sedimentation and global transport by the mesospheric meridional circulation (e.g. Rosinski and Snow, 1961; Hunten et al., 1980; Kalashnikova et al. 2000; Gabrielli et al., 2004; Megner et al., 2006; 2008a; 2008b). The general circulation of the atmosphere transports the MSPs away from the summer pole towards the winter pole and into the polar winter vortex (Megner, 2007; Bardeen et al., 2008; Megner et al., 2008a; 2008b), thus producing a strong annual variation. The general composition of the meteoric smoke material is thought to reflect the composition of the incoming meteorite material. However, due to differential ablation processes and the altitude-dependent chemical environment, the detailed smoke composition is expected to depend on the history of the individual meteoric particles (e.g. McNeil et al., 1998; Kalashnikova et al., 2000). Considering the meteoric influx, major vapour components are presumably silicon, iron and magnesium, with minor contributions from other metals like sodium, aluminium, potassium, calcium, lithium etc. Following gas phase chemical transformation prior to re-condensation, these compounds are likely to be present in the form of oxides,

hydroxides and carbonates in the resulting smoke particles (e.g. Plane, 2003; Self and Plane, 2003; Plane and Whalley, 2012).

Basic information about MSP properties is today available from optical occultation measurements (Hervig et al., 2009, 2012) and, more indirectly, as a fraction of the particles is expected to be charged by the surrounding plasma, from measurements of heavy charge carriers from sounding rockets (Schulte and Arnold, 1992; Havnes et al., 1996; Gelinas et al., 1998; Horányi et al., 2000; Croskey et al., 2001; Robertson et al., 2004, 2009, 2013; Lynch et al., 2005; Barjatya and Swenson, 2006; Smiley et al., 2006; Havnes and Næsheim, 2007; Amyx et al., 2008; Strelnikova et al., 2009; Rapp et al., 2005, 2010, 2012; Havnes et al., 2013), and from incoherent scatter radars (Rapp et al., 2007; Strelnikova et al., 2007; Fentzke et al., 2009). Experimental studies have been performed in the laboratory (Saunders and Plane, 2006; 2011), but much of the existing knowledge about MSPs relies on model results (e.g. Hunten et al., 1980; Megner et al., 2006, 2008a, 2008b; Bardeen et al., 2008). It has been shown that substantial amounts of particles of meteoric origin are present in the stratosphere (e.g. Murphy et al., 1998; Cziczo et al., 2001) and that meteoric smoke particles reach the Earth´s surface (e.g. Gabrielli et al., 2004; Lanci and Kent, 2006; Dhomse et al., 2013), but no equivalent measurements of particles have ever been achieved in the mesosphere. Attempts were made in the 1960s to sample mesospheric aerosol from sounding rockets (e.g. Hemenway et al., 1964; Soberman and Hemenway, 1965; Farlow et al, 1970), but none of the measurements resulted in any conclusive results. Very recently, a student experiment attempted to sample particles from a sounding rocket launched within the REXUS/BEXUS (Rocket/Balloon Experiment for University Students) programme, a bi-lateral cooperation between the Swedish National Space Board (SNSB) and the German Aerospace Center (DLR), but results from the analysis is not yet available (see Reid et al. (2013) for details about the experiment).

Although there is only indirect evidence of their existence in the mesosphere, MSPs have been proposed as a key player in the formation and evolution of several observed mesospheric phenomena. Smoke particles are today recognised as the most likely candidate for condensation nuclei for mesospheric ice particles (Rapp and Thomas, 2006) and hence phenomena such as noctilucent clouds, NLC

(Gadsden and Schröder, 1989; Thomas, 1991), or polar mesospheric clouds, PMC, and polar mesosphere summer echoes, PMSE (Rapp and Lübken, 2004). These water ice particles (Hervig et al., 2001) are probably not pure ice with just one MSP as nuclei, but more likely "dirty" ice particles with a large amount of MSPs embedded in them along with metal atoms and molecules from meteoric ablation (Havnes and Næsheim, 2007; Hervig et al., 2012; Kassa et al., 2012; Havnes et al., 2013). Smoke particles are also believed to be responsible for the polar mesosphere winter echoes (PMWE) observed by radars outside the PMSE season (e.g. Zeller et al., 2006). With the advent of more powerful radars, these winter echoes have now been observed also during summer below the much stronger PMSE (Latteck et al., 2012). Heterogeneous chemistry has been suggested to take place on the surfaces of smoke particles. An example is the proposed catalytic recombination of O and H_2 as a local source of water vapour in the mesosphere to explain observations of mesospheric HO_x chemistry and unexpectedly high water concentrations (Summers and Siskind, 1999; Conway et al., 2000). By scavenging various gas-phase products of meteoric ablation, MSPs are thought to act as a sink in mesospheric metal chemistry (Plane, 2004). Smoke particles can also efficiently scavenge free electrons and ions and can thus play a substantial role in the D-region charge balance (Rapp and Lübken, 2001; Rapp, 2009; Friedrich et al., 2011). This charging may in turn strongly affect smoke coagulation and ice particle nucleation processes (Gumbel and Megner, 2009; Megner and Gumbel, 2009). The strong downward circulation in the winter polar vortex can efficiently transport MSPs down into the winter stratosphere. Here, MSPs can be involved in stratospheric chemistry and the microphysics of polar stratospheric clouds (PSC) and thus have important effects on ozone chemistry (e.g. Murad et al., 1981; Curtius et al., 2005; Voigt et al., 2005, Saunders et al., 2012). Very recently Dhomse et al. (2013) predicted high deposition of MSPs to occur at middle latitudes, providing a significant source of Fe fertilization to the Southern Ocean.

Despite their apparent importance, little is known about the properties of meteoric smoke particles and none of the hypotheses above can be verified without direct evidence of their existence, altitude and size distribution, and composition. The objective of the MAGIC project (Mesospheric Aerosol – Genesis,

Interaction and Composition) was to quantitatively answer fundamental questions about the properties of MSPs in the mesosphere:

- Do re-condensed smoke particles of meteoric origin exist in the mesosphere?
- What is their number density, shape and size distribution?
- What is their spatial distribution and how are they transported?
- What is their elemental and molecular composition?
- How do they interact with their mesospheric and ionospheric environment?

To address these questions, an instrument was designed and built to directly sample meteoric smoke particles in the mesosphere and return them to the ground for detailed laboratory investigations. In this paper we describe the MAGIC meteoric smoke particle sampler and present attempts to directly sample MSPs. In section 2 the ideas behind the MAGIC project are presented and the MAGIC sampler is described in detail. Section 3 then describes the measurement campaigns and results are presented and discussed. Section 4 provides a summary and conclusion with some thoughts for the future.

2. The MAGIC Idea

2.1 The challenge

In order to understand the role of meteoric smoke particles in the mesosphere and their impact on that environment their presence must be certified and their physical characterization (number density, size distribution, shape, composition etc.) determined. The *in situ* detection of neutral nanometre-size particles is however very difficult. They are too small for optical detection and their momentum is not sufficient to produce electrical pulses upon impact. A way to obtain maximum information about particle properties is by direct collection followed by detailed laboratory analysis. However, the sounding rocket approach, which is the only practical method to carry out a sampling experiment at mesospheric altitudes, is subject to critical limitations imposed by aerodynamics. As nanometre size particles tend to follow the airflow around the

rocket payload structure rather than reaching the detector surface, their sampling is a substantial experimental challenge and careful aerodynamic design is of critical importance for smoke particle experiments. The interpretation of the particle measurements also requires a detailed understanding of the specific detector response, which is far from trivial. Basic questions are e.g. how measured particle concentrations and properties are related to the particle concentrations and properties in the undisturbed atmosphere.

Around the turn of the century, significant progress was made in the analysis of aerodynamic influences on sounding rocket measurements (Gumbel et al., 1998; Gumbel, 2001) and the fate of atmospheric particles approaching a rocket detector (Horányi et al., 1999; 2000). Based on these results, the fundamental concept of the MAGIC instrument design was to minimize the aerodynamic perturbations by the use of a small sampling probe extending forward of the rocket payload. By using a collection surface of 3 mm diameter, the sampling probe dimension is reduced to the order of the molecular mean free path, which minimizes flow effects on incident particle trajectories in the vicinity of the probe. In order to characterize the sampling process, Hedin et al. (2007b) performed simulations of the trajectories of nanometre-sized dust particles towards the MAGIC detectors with a statistical particle motion model for the conditions of the first rocket launch at Esrange in January 2005. An important feature of this model is the Brownian motion of the particles due to thermal collisions of the gas molecules (Hedin et al., 2007a). Figure 1 shows trajectories of simulated particles of 0.4, 0.6 and 0.8 nm radii towards the MAGIC sampling surface at an altitude of 80 km for the conditions of the Esrange 2005 flight (but with a zero degree angle of attack). The flow is from the left and the grey scale is the air number density normalized to the unperturbed free-stream conditions. It can be seen here that even particles as small as 0.4 nm radius will impact on the sampling surface at this altitude. As a result from this simulation, a detection efficiency for the MAGIC detector as a function of altitude and particle size is obtained (Fig. 2). These simulations confirm that particles of radii down to 0.75 nm impact on the sampling surface with an efficiency exceeding 80% over the entire mesospheric altitude range of interest.

2.2 The MAGIC sampler

The MAGIC detector concept was developed in collaboration between the Naval Research Laboratory (NRL) in Washington D.C. and German and Swedish scientists (Gumbel et al., 2005) and four MAGIC collection instruments were built at NRL. In collaboration with the Department of Meteorology at University of Stockholm (MISU), the first flight of the MAGIC collectors took place on a rocket launched at Esrange Space Center, Sweden, in January 2005 (the MAGIC campaign). The second flight was in collaboration with the Virginia Polytechnic Institute and took place in May 2005 with a launch at Wallops Island, USA. In September 2006, August 2007 and June/July 2008 MAGIC collectors were launched as part of the German-Norwegian ECOMA project at Andøya Rocket Range, Norway. The last flight of a MAGIC collector was on the Swedish PHOCUS campaign at Esrange, Sweden, in July 2011.

As the rocket payload transits the mesosphere, the MAGIC collector sequentially extends a number of sampling probes at specific altitude windows. On the exposed face of the probes, transmission electron microscopy (TEM) grids were mounted to collect particles in a directly analysable form, thus minimizing the risk of particle loss and contamination. Up to nine sampling pins (of which at least one is used as reference, i.e. not exposed to the atmosphere) are mounted in a revolver mechanism (Fig. 3). This pin-revolver mechanism is driven by a worm gear, which allows sequential positioning of the pins with high precision under the pin exit hole of the revolver-chamber. Once in position, a chain drive mechanism is used to extend a piston, which pushes the collection pin upward through the exit hole in the top of the MAGIC instrument (Figs. 4 and 5). Particles that impact the TEM grid while extended outside of the MAGIC instrument are expected to stick by van der Waals forces. After a few seconds the pin is retracted back into its original position in the pin-revolver. A pair of permanent magnets provides the necessary coupling of the extension piston to the sampling pin, so that the sampling pin can be retracted into the revolver. The extension piston detaches from the magnet when the collection pin is completely back in its compartment in the revolver. The worm gear then drives the pin-revolving mechanism so that the next pin can be extended. In this way dust from specific

altitude intervals in the mesosphere can be analysed when the TEM grids are returned to Earth.

The pin exit hole is opened by removing a vacuum plug that is used to seal the exit hole during launch. This plug mechanism is controlled by a rod, which is extended through the pin-revolver mechanism's axis. This rod is driven by a lead-screw that lifts the plug out of the exit hole. The plug is then rotated with the revolver mechanism, until it returns to its original position at the end of the sampling sequence near the apogee of the flight. At this point the plug is reinserted to vacuum seal the chamber thus preventing water or other contaminants from entry into the MAGIC instrument on landing.

Nominally the MAGIC collection system is completely self-contained, i.e. it has it own power supply (rechargeable batteries), microprocessor and requires no telemetry. A signal is sent from the rocket service module at a pre-set time after the launch to start the sampling sequence as programmed in the microprocessor. For the purpose of real time monitoring of the MAGIC instrument during flight, two signals have been transmitted by telemetry, (1) pressure inside instrument and (2) status signal indicating when a collection pin is in the extended position. Monitoring of these two signals during flight and subsequent instrument checks are performed to confirm that the instrument functioned as expected. After the ECOMA campaign in 2006, the electronics were remodelled and the internal power supply was removed. From then on, the MAGIC samplers were powered from the rocket service module.

2.3 Sampling surface

The appropriate choice of collection surface for nanometre-size particles is crucial. With regard to the anticipated laboratory analysis, the use of carbon film coated TEM grids as sampling surfaces has been the primary choice. An important benefit of using TEM grids as sampling surfaces, is that additional post flight treatment of collected particles, such as separating and moving the nanometre size particles from the sampling surfaces is not required.

Two experimental investigations have been made to test the sticking efficiency of the TEM grids for nanometre size particles (Reissaus et al., 2006). Using a molecular-beam apparatus at the University of Jena, Al_2O_3 and C particles of a

few nanometres were produced at speeds of 1 km/s. The laboratory impact experiments demonstrated that nanoparticles, both as single particles and fractal agglomerates, do stick on carbon surfaces after high velocity impacts with moderate efficiency (14%) for Al_2O_3 and moderate to high efficiency (24–83%) for C. The higher collection efficiency for C particles may be due to that they chemically bind to the C on the TEM grids. Unfortunately, the relevance of these numbers for the mesospheric MAGIC measurements remains unclear as the overall sticking probabilities determined in the laboratory may be dominated by large agglomerates of nanometre particles that were formed in the molecular beam prior to impact on the grids. As an additional finding, the experiments confirmed that at speeds of the order of 1 km/s the particles do not penetrate the carbon film on the TEM grid. These experiments were made with a 0° angle of attack, i.e. the particles impacted the surface with normal incidence. At angles of attack of 10-20° or larger, which is typical for sounding rocket experiments without attitude control, the sticking efficiency will be different (most likely smaller).

Other probe materials have been considered during the development of the measurement concept, most notably aerogel. While sticking probability in the aerogel matrix is close to unity, the difficulty in removing nanometre particles from the aerogel for electron microscopy analysis made the choice of this material not feasible. On 16 November 2012, a student experiment was launched on a sounding rocket from Esrange Space Center within the REXUS/BEXUS program with the objective to collect particles in the mesosphere and stratosphere. The sampling probes contained collection surfaces of three different types: standard TEM grids, glass fibre filter paper, and silicone gel (Reid et al., 2013). Results from the analysis of these surfaces are not yet available.

2.4 Measurement procedure

In the preferred payload configuration at least two MAGIC collectors are used where the instruments alternate the sampling pin extension to ensure that there are no gaps in the sampling procedure. Before flight the instruments are carefully prepared in a clean room environment. By using specific mounting tools, care is taken so that the part of the TEM grid used as collection surface is

not in direct contact with any other surface. On every flight, each MAGIC instrument had (at least) one collection pin with a TEM grid that was only to be used as a reference surface and that was therefore never extended during the collection sequence. This unexposed reference TEM grid is attached and removed together with the ordinary TEM grids used in the collection sequence. Any contamination from the instrument itself or from TEM grid mounting and removal procedures will thus be detected on this reference grid. Once the sampling procedure during flight is completed the MAGIC unit closes the vacuum seal and is kept under the low vacuum acquired during the time of the sampling operation in the mesosphere. After the recovery of the payload, the MAGIC instruments are kept under vacuum until the first examination of the TEM grids. To avoid the use of additional transfer or storage containers before the first examination of the reference and collection surfaces, the TEM grids can be removed adjacent to the transmission electron microscope. In this way, once a grid is removed from the MAGIC instrument, it can be mounted immediately in the transmission electron microscope.

It is important to note that the small collector dimensions are a decisive difference between the current approach and efforts to sample NLC particles in the 1960s [e.g., Hemmenway et al., 1964a; Farlow et al., 1970]. The aerodynamic conditions for these large earlier collectors a priori prevented a detection of particles in the nanometre size range. In addition, the smallness of the MAGIC collection system concept is a precondition for efficiently keeping sampling surfaces clean and under vacuum.

2.5 Data analysis

The analysis of the MAGIC smoke samples after recovery is primarily based on detailed transmission electron microscopy (TEM) studies mainly at the Materials Science and Technology Division of NRL and, since 2008, at the Electron Microscopy Centre (EMC) in the Department of Materials and Environmental Chemistry at Stockholm University. The TEM analysis is intended to provide particle numbers, sizes and shapes, while the combination of the TEM technique with energy-filtered imaging and energy-dispersive x-ray spectroscopy (EDS or EDX) can provide the elemental composition of the sampled particles. Imaging

and compositional analysis studies were performed using a JEOL JEM-2200FS 200-kV (NRL) and a JEOL JEM-2100F 200-kV (EMC) field emission scanning TEM (STEM), with an EDX system and high-angle annular dark-field (HAADF) imaging capability. The grids were imaged in conventional bright-field and HAADF modes to determine particle sizes, shapes and number density.

Energy filtered images can be obtained by selecting only the transmitted electrons that interact inelastically with the sample and thus exhibit an energy loss characteristic of the elements present in the sample. The energy-filter window can be tuned to a specific elemental edge so that the image intensity directly reflects the concentration of the chosen element. Advantages with this technique are that it is sensitive to light elements including C, N and O, and that it is relatively fast. EDX can then determine the quantitative elemental and molecular composition. EDX analysis utilizes the characteristic x-ray fluorescence emission from the sample due to absorption of energetic electrons to accurately determine the sample composition. Elements as light as boron can be detected while quantitative results are obtained for carbon and heavier elements. These measurements are more time intensive than energy-filtered imaging, but can be used to determine the composition of the particle to less than 0.01 atom %, if appropriate calibration standards are used.

3. Results and discussion

3.1 First flights

There were two flights of MAGIC instruments in 2005. The first took place in the MAGIC sounding rocket campaign at 04:37 UT (05:37 LT) on January 10 from Esrange Space Center, Sweden (68°N, 21°E). On this flight three MAGIC collection instruments were flown along with the Hygrosonde water vapour instrument (Khaplanov et al., 1996; Lossow et al., 2008) and two charged aerosol detectors (Gumbel et al., 2005; Amyx et al., 2008). As can be seen in Fig 4, the three MAGIC instruments were mounted symmetrically around the centrally located Hygrosonde. Continuous 30 nm carbon film coated Cu TEM grids (Fig. 5a) were exposed between 59 km and the apogee of 95 km. The second flight took place on May 17 from Wallops Island, Virginia (38°N, 75°W) as part of the Virginia

Tech Student Sounding Rocket Project (VTSRP). One MAGIC collector was flown on this flight (Fig. 6), which reached an apogee of 98 km. Three pins with ultra thin 3 nm continuous carbon film on a holey carbon film (or carbon mesh) coated Cu TEM grids (Fig. 5b) were exposed between 70 and 97 km (in Fig 5b, the holey carbon film or carbon mesh is the dark grey net supporting the light grey ultra thin continuous carbon film).

Technical issues associated with the collection TEM grids hampered initial results from the Esrange grids. The 30 nm thick continuous carbon film resulted in low contrast between the film and the collected particles. Hydrocarbon build up during TEM analysis reduced the contrast even further, which consequently made the analysis more difficult. In spite of this, HAADF images show particles in the 1-10 nm radius size range. Figure 7 shows particles found on the Esrange grids. Panels a) to d) in Fig. 7 are images of the grids exposed at altitudes between 86.3 and 94.5 km, where panel a) shows a high-resolution bright-field image and the other three are HAADF images. Panels a) and b) are images of the same region. EDX spectra show weak signal from Si. The square patterns with reduced contrast in panels c) and d) show the effect of the thin film of hydrocarbons present on the grid. The reference grids do not show any of these nanometre-sized particles, but their origin is not known. Larger particles were seen on both exposed (panels e) and g), exposed at 90.3-94.3 and 93.3-94.5 km, respectively) and reference grids (panels f) and h)) and are likely contamination. The large particles shown in panels e) and f) contain Ti, Si, Na, K, Ca and Al, while the particles in panel g) and h) contain Fe, Si, Al, Ca and Cr. The two on board Colorado dust detectors (CDDs) indicated particles in the altitude range 79 to 85 km (Amyx et al., 2008) which was covered by pins three and four of each of the three MAGIC samplers, as can be seen in Fig. 8.

For the Wallops flight a switch was made to a new type of TEM grid with a carbon film thickness of only ~3 nm, about ten times thinner than the Esrange grids. These new TEM grids gave a much-improved contrast, but came with the disadvantage of the presence of some silica left from the manufacturing process. All of the TEM grids from 2005 reveal nanometre particles, however, the imaging contrast is best on the 3 nm thick regions of the Wallops flight grids shown in Figs. 9 to 11. For presentation purposes of the grey-scale raw HAADF images

were converted to colour using the colour gradient tool in Photoshop CS. This transformation retains the intensity information of the raw images, in which contrast is directly proportional to variation in sample thickness and depends inversely on the square of the atomic number density of the sample. Based on the 1% area analysed, several distinct classes of particles types could be identified.

The most common morphologies are clusters, 10 nm to several microns across, comprised of aggregated particles of 0.5-2 nm in radius (Fig. 9), which in the EDX spectra appear to be primarily Si and O. The HAADF images show a range of 10-50% coverage of the grid film with clusters, corresponding to approximately 10^4-10^5 particles μm^{-2} in the 0.5-2 nm range, and an atmospheric abundance of 10^6-10^7 cm^{-3}, assuming 100% collection efficiency. The images indicate a sharp drop-off in abundance for particle >2 nm. However, due to the presence of silica left from the manufacturing process, it is not possible to show that these particles were collected during flight.

Other particle morphologies occur at orders of magnitude lower abundance (see Fig. 10) than the 0.5-2 nm radius particles. These include isolated 2.5-5 nm radius particles, holes produced by particles that breached the support film, particle rings, 25-125 nm monolithic particles, and micrometre-sized particles and aggregates. The isolated 2.5 - 5 nm particles are dense spheres with varying concentrations of Si, O, Ca, Al, Fe, and S, consistent with material of meteoric origin. The holes (vertical arrows, Fig. 10), presumably produced by particles that breached the support film, are 25-75 nm in radius and are rimmed with material; possibly peeled back carbon film. The particle rings (angled arrow in Fig. 10, and Fig. 11) have a diffuse circular perimeter that is sometimes studded with high-density aggregates. Monolithic particles ranging from 25-125 nm in radius appear to be individual mineral grains, composed e.g. of silicates and magnesium aluminium oxides, and faceted surfaces consistent with an origin as matrix materials from incompletely ablated micrometeorites. There are also of the order of 10 particles per collection grid in the micrometre size range. These are most likely contamination, as the presence of particles of this size is common in the terrestrial environment, even in the clean room environment of the microscope laboratory. However, some of these large particles have

compositions and morphologies consistent with an origin as meteoroid fragments or interplanetary dust particles (IDPs).

The unexpectedly diverse morphologies of the collected material present some questions that have not yet been resolved. The different morphologic groups must result from diverse origins and atmospheric processes. The fact that the most abundant particles observed are in the 0.5-1.5 nm size range is generally consistent with expectations (e.g. Hunten et al., 1980; Kalashnikova et al., 2000; Bardeen et al., 2008; Megner et al., 2008b), i.e., an exponentially decreasing particle abundance with increasing size. However, the absolute abundance observed ($>10^6$ particles cm^{-3}) is greater than predicted by the atmospheric models by one or more orders of magnitude. The clustering of the particles into what appears to be porous clusters, or fluffy aggregates, was not considered in the above models (e.g. Hunten et al., 1980; Kalashnikova et al., 2000; Bardeen et al., 2008; Megner et al., 2008b). It is unclear what the high surface area of the fluffy aggregates will do to their aerodynamic and chemical properties, e.g., settling times and surface reactivity, as this will depend on the mass of the three dimensional particle and it surface area. It is possible that the clustering into fluffy aggregates occurred on the sampling grids rather than being created in the atmosphere.

The less abundant particle morphologies require separate explanation. The spherical 2.5-5 nm radius particles could represent the upper end of the size distribution of individual condensates of ambient ablated meteoritic materials. Their larger size causes a faster settling rate and less time for incorporation into aggregates, which may explain their isolated occurrence. The 75-150 nm diameter holes in the 3-nm thick carbon support films may be produced by dense particles rather than fluffy aggregates. These particles are possibly the same type of particles as the observed 25-125 nm dense monoliths. The material in the rims around the holes could be small grains adhered to the surface of the monoliths that were collected on the film as the monoliths breached the film. Alternatively, the material in the rims could result from deformation of the carbon support film at the breach. The holes are observed on the 76.7–93.5 km and 94.5–97.0 km Wallops collection grids. The rings (see Fig. 11) appear to result from the evaporation of a liquid. During evaporation, the surface tension

of the liquid concentrated inclusions of sub-nm to 1.5 nm particles at the perimeter, producing the diffuse ring. This phenomenon is commonly observed during TEM analysis of solvent-dispersed synthetic nanoparticles. In the present case, the source of the liquid is not obvious; melting of a solid particle upon impact or upon return of the rocket to Earth are possibilities. No residue was found on the TEM grid that would readily allow the determination of the composition of the incident particle. Water ice particles are considered very unlikely as atmospheric temperatures at the collection altitudes are well above the ice sublimation point. In the cases for which large particulate agglomerates are observed at the perimeter, it appears most likely that these agglomerates were deposited by the incident particle as it liquefied, since adjacent regions of the support film do not contain particles of this size.

It must be remembered that observations reported here stem from only a limited 1% study of the returned data. When additional studies were to be performed after some time on the Wallops grids and lower altitude Esrange grids, the TEM carbon film had broken in many places during the storage and further analysis was not possible.

3.2 ECOMA

In 2006, 2007 and 2008, MAGIC was launched within the ECOMA program (ECOMA = Existence and charge state of MSPs in the middle atmosphere) from the North-Norwegian Andøya Rocket Range (69°N, 16°E). The ECOMA project was an international research program led by the Leibniz-Institute of Atmospheric Physics (IAP) in Germany and the Norwegian Defence Research Establishment (FFI) in Norway and brought together scientists from Germany, Norway, Sweden, Austria, and in 2008 also from the USA. The general objective was the study of MSPs and their relationship to ionospheric processes (Strelnikova et al., 2009; Rapp et al., 2010, 2012).

The main instrument on board the payloads was the ECOMA detector from IAP; a classical Faraday cup detector combined with a Xenon flash-lamp for the active photo-ionization/photo-detachment of MSPs and the subsequent detection of resulting photoelectrons (Rapp and Strelnikova, 2009). During all three campaigns, *in situ* measurements of neutral density, temperature and turbulence

were provided by IAP, and ionization conditions were studied in terms of ionospheric composition and turbulence by the Technical University Graz, Austria, and FFI. Figure 12 shows the front deck configuration (under the nosecone) of the ECOMA payloads. Both the 2007 and 2008 campaigns were conducted during the NLC season and the presence of ice particles was monitored by on-board NLC photometers from MISU. In 2008 additional detectors for charged particles were flown by Dartmouth College, USA, and the University of Tromsø, Norway. The rocket-borne measurements were complemented by the comprehensive ground-based instrumentation at Andøya Rocket Rage, in particular the ALOMAR lidars and radars, as well as the EISCAT radar facility.

3.2.1 ECOMA 2006 Campaign

The 2006 ECOMA campaign was planned to feature three launches with two MAGIC detectors on each payload (Fig. 12a-b). The four MAGIC instruments were jointly prepared by NRL and MISU. In an attempt to clean the grids from Si and other contamination in the carbon film, the grids were treated at NRL with a chemical etching using a gas mixture of CF_4 and Ar under plasma cleaning conditions. After this the grids were oxidized by plasma cleaning in an atmosphere of O_2 and Ar. The first payload and set of two MAGIC detectors were to be refurbished and launched a second time as launch number three. The ECOMA-01 payload was launched on September 8, 2006 at 22:17:00 UT (LT = UT + 2 h) and reached an apogee of 130.6 km. All instruments performed nominally and the two on-board MAGIC instruments performed the sampling sequence with 7 pins each covering more or less the entire altitude region from 68 to 116 km. The ECOMA detector measured photoelectrons from the photo-ionization/photo-detachment of MSPs from 80 km altitude on the ascent (Strelnikova et al., 2009). The TEM grids used on this flight were the same type of TEM grids that was used on the earlier MAGIC campaign at Esrange (continuous 30 nm carbon film on a 200 lines/inch Cu mesh). The chemical etching of the carbon film before flight also made the carbon film thinner thus improving the contrast and making it possible to see smaller particles.

The ECOMA-02 payload was launched nine days later on September 17, 2006 at 21:06:45 UT and reached an apogee of 130.3 km. The two on-board MAGIC instruments sampled the atmosphere from 68 to 120 km altitude using the same type of grids as was used on the Wallops Island launch in 2005 (ultra thin carbon film on a holey carbon support film and Cu mesh). Unfortunately, this payload was lost to the bottom of the sea due to a malfunction of the payload recovery system, and consequently two MAGIC collectors were lost and analysis of these grids was not possible. This malfunction led to the premature termination of the 2006 campaign to investigate the failure and hence, no third launch was carried out.

The ECOMA-01 MAGIC sampling grids all suffered from heavy contamination. In addition to the film-like hydrocarbon contamination that was seen on the grids from the 2005 MAGIC campaign there were hydrocarbon blobs: dark, opaque, roundish blobs and lighter, irregularly shaped blobs with central dark spot (Fig. 13a-b). Also “snow flake” shaped hydrocarbon contamination was seen (Fig. 13c). The EDX data of the hydrocarbon contamination showed abundance of C and F which is consistent with the lubrication used on the O-rings in the MAGIC housing. So the source of the thick hydrocarbon contamination was most likely vaporising of the O-ring lubricant and melting of the O-rings near the pin exit hole during re-entry into the denser atmosphere. On ECOMA-01 the MAGIC samplers were mounted in a less protected manner than in the two flights in 2005 and, hence, where more susceptible to air frictional heating during re-entry (see Fig. 12a-b).

Although the hydrocarbon contamination made EDX difficult, abundant spherical particles with radii in the 0.5-5 nm size range were also found on the ECOMA-01 MAGIC grids. The most abundant type was Fe-rich particles composed of Fe and Cr with some Ni and Mo. Cr, Ni and Mo are common components of stainless steel, but Mo has a very low abundance in meteoritic material. Also the Cr content (~10-20%) was much higher than what is found in chondrites, or expected in meteoric smoke particles, but consistent with stainless steel. This indicates that these particles are stainless steel and thus most likely contamination. As opposed to the hydrocarbon contamination, the source of the stainless steel particles has never been identified. Several EDX measurements

were performed of the composition of suspect parts used in the MAGIC sampling unit and the ECOMA detector, but none of the parts contained Mo. The conclusion was that the stainless steel particles do not come from the MAGIC units, nor from the ECOMA detector, but must come from somewhere on the rocket. A possible explanation was the presence of nanosize steel spheres in a lubricant applied in the payload's nosecone separation system. It is also possible that the rocket motor passed the payload after separation due to aerodynamic effects or afterburning. This has happened in some cases in the past, which means that the motor ends up upstream of the payload and all kinds of debris will reach the payload. The first MAGIC grid was exposed between 68 and 73 km while the motor was separated later, at an altitude of 75 km. The second and third TEM grids of that same MAGIC instrument was exposed after the separation (between altitudes 78 and 86 km, and 89 and 93 km, respectively) show at least an order of magnitude more particles per unit area than what is seen on the first grid (see Fig. 14). The second MAGIC instrument exposed its first TEM grid between 78 and 82 km and has the same amount of particles as the subsequent second and third grids. This is consistent with the idea that the contamination could come from the motor. However, even though the grid exposed before motor separation shows much less particles, there were still stainless steel particles with Mo on this grid. Also the reference grids show abundant nanometre sized stainless steel particles containing Mo. The top ring of the front deck of the ECOMA payload (onto which the nosecone is mounted, see Fig. 12a) is made of stainless steel that does contain Mo. It is however not known what process would produce nanometre-sized particles from this surface. If the particles were exclusively from the atmosphere, and assuming a 100% sticking efficiency, the amount of particles on the first, second and third grids of the second MAGIC sampler would correspond to an atmospheric number density of $\sim 1.5\times10^{4}$ cm^{-3} for particles of radius 1 nm and larger (a factor of about two orders of magnitude smaller than for the Wallops Island flight). The second most abundant type of particles was larger in size (~50-100 nm radii) and contained Ca and S with K and/or Na (or possibly Zn). The source of these is not known. No signs were found of ring structures or holes in the film similar to what was seen on the Wallops Island flight.

After the 2006 ECOMA campaign, O-rings and lubricant were changed to more heat resistant types. Also an extension to the MAGIC instrument was added to protect the pin exit hole and the volume around it from the possible airflow through the ECOMA detector (see Fig. 12c). These extensions also served as heat shields of the upper MAGIC housing during re-entry.

3.2.2 ECOMA 2007 Campaign

Similar to the 2006 ECOMA campaign, the 2007 campaign was planned to feature three launches with two MAGIC detectors on each payload. On August 3, 2007 at 23:22:00 UT the ECOMA-03 payload was launched and reached an apogee of 126 km. Unfortunately, also this payload was lost to the bottom of the sea due to a malfunction of the payload recovery system. The decision was made to terminate the campaign prematurely to investigate the malfunction, and return in 2008. Now all four MAGIC collectors originally manufactured at NRL had been lost. Thanks to the efforts of NRL, MISU and DLR Moraba, two new MAGIC samplers could be built mainly from spare parts.

3.2.3 ECOMA 2008 Campaign

MAGIC particle samplers were flown on three payloads during the ECOMA campaign in June/July 2008. One MAGIC instrument for each rocket payload was jointly prepared by NRL and Stockholm University, again with the first payload and MAGIC collector to be refurbished and launched a second time. The three launches (ECOMA-04, -05 and -06) took place on June 30 at 13:22 UT, July 7 at 21:24 UT, and July 12 at 10:46 UT, respectively (LT = UT + 2h). The payloads performed nominally and were successfully recovered by boat after the water landing. The scientific conditions for all flights were interesting. All three went into NLC ice particle layers as confirmed by the on-board photometers from Stockholm University. For the first and third flights, sampling was performed below (one grid), within (one grid) and above (two grids) the NLC on each flight. On the second flight, the opening of the extension of the first pin was delayed for some unknown reason and the sampling started inside the NLC. Two additional pins in each MAGIC collector were prepared with grids and used as reference (i.e. not extended). Strong polar mesosphere summer echoes (PMSE) were present

during the first and third flight and completely absent during the second. The ECOMA detector reported the presence of particles above 77 km for ECOMA-04, above 81 km for ECOMA-05, and above 70 km for ECOMA-06 (Rapp et al., 2010). Above 90-95 km the ECOMA photoelectron measurement is most likely contaminated by photoelectrons from the photo-ionisation of NO (Rapp and Strelnikova, 2009; Rapp et al., 2012).

The TEM grids used for these flights were the 30 nm continuous carbon film on Cu support grids also used earlier. Also this time the grids were pre-treated at NRL to reduce Si and other contaminants and to improve the contrast by making them thinner. The grids were then characterised at Stockholm University before launch to determine the quality of the carbon film, the number of particles and their chemical composition. This analysis was made in the four central squares of each grid and in one grid that is covered by the Cu masks (Fig. 15a). The grid square covered by the Cu mask was used as an on-grid reference area. This characterisation was then used to rank the quality of the TEM grids and to determine which ones should be mounted in the MAGIC collector. The same analysis was then also made after the flights. The set of six TEM grids from the ECOMA-04 flight was analysed at Stockholm University, while the two sets from the ECOMA-05 and -06 flights were directly shipped back to NRL for analysis.

During the pre-flight analysis, the only elements that could be observed in the carbon film above the detection limit were C (film and some flakes), O, F, Si (particles smaller than 5 nm) and Cu. F and possibly O originate from the plasma cleaning process, while Si is still some contamination left from the grid manufacturing process also after the plasma cleaning. The Cu signal originates from the fluorescence of the surrounding support grid and possibly from deposition onto the film by the plasma cleaning process. In STEM-HAADF mode small particles could be observed that by spot measurements give EDX spectra that locally indicate high concentrations of the elements Na, Al, Mg, Si, Cr, Mn, Fe and Ni. After the launch the same characterisation was performed on the ECOMA-04 grids at Stockholm University. Table 1 summarizes the elemental composition analysis of the TEM grids before and after launch. The conclusions from this characterisation are that the grids survived almost intact with no serious damage to the carbon film, and that the overall chemical composition of

the carbon film was the same, with the exception of an increase of Cu and a reduction of O (highlighted with red squares in Table 1). There were no signs of hydrocarbon contamination or stainless steel particles on any of the grids. Hence, the change of O-ring lubricant and the addition of the extension as a protection and heat shield after the ECOMA-01 launch helped. However, no flight-sampled nanometre-sized particles could be identified.

The increase of Cu on the carbon film is significant, and it increases with altitude. However, the highest concentrations are observed on the reference grids that were not exposed. The increase in Cu content is seen as an addition of small sub-nanometre to nanometre particles onto the carbon film. Except on the first grid, the oxygen content of the carbon film decreases significantly with exposure altitude, including the reference grids. The concentrations of the other elements were more or less constant. A large number of STEM-HAADF images of the carbon film were recorded with the aim to calculate the number of collected particles and their sizes. The general observation was that with increasing Cu content the number of particles also increased. This causes a problem in identifying smoke particles by EDX as the noise from the Cu contamination drains the signal from the other elements.

On the grid that was exposed when the payload passed through the NLC layer, large spherical agglomerates (radii ~0.5 - 0.8 μm) were found after the flight. Energy filtered imaging (Fig. 16) shows that they contain Na, S, Si and O with some Cl, K, Ca, Mg, Cr, Mn and Fe in both the centre and outer parts of the agglomerated material. The number of such agglomerates was estimated to about four in each of the four central squares. Similar agglomerates were, however, also found on the reference square under the Cu mask (Fig. 17a). The Cu mask was not mounted completely flush to the TEM grid, so there is a possibility for particles to enter in the space between them and end up on a grid square under the mask. More careful studies showed appearance of this type of particles also on the two unexposed reference grids (Fig. 17b-c). It is possible that, even if they were not observed before flight, they could have been there from the beginning. These agglomerates are very similar in shape and size to the patterns seen on the surfaces exposed to NLC in the 1960s (Hemenway et al., 1964b; Skrivanek and Soberman, 1964). If these agglomerates are NLC particles

from the 1 km thick ice layer as seen by the on-board NLC photometer, the number density derived from the second grid is 0.5 cm^{-3} (if the sticking efficiency is 100 %). This is a factor of about two orders of magnitude smaller than for typical NLCs (e.g. von Cossart et al., 1999; Baumgarten et al., 2008).

The grids from ECOMA-05 and -06 that were shipped to NRL were not in the same good condition when they arrived as the grids that were analysed at Stockholm University. There were many places were the carbon film had ruptured, and this most likely happened during transport. An attempt was made to calculate the number of nanometre sized particles and their size distribution on the ECOMA-06 grids. The results are summarised in Table 2 and from this it can be seen that the particles on all grids are almost identical, with similar mean radius and spread. The atmospheric particle number densities calculated assuming 100% sticking efficiency are several orders of magnitude higher than what is expected from models for particles of this size and for polar summer conditions (Megner et al., 2008a). This all suggests that these particles are in fact contamination.

3.3 PHOCUS

The last flight of a MAGIC sampler was on the PHOCUS sounding rocket launched from Esrange Space Centre, Sweden, on July 21, 2011, at 07:00:53 UTC into a strong NLC. PHOCUS, which is an acronym for Particles, Hydrogen and Oxygen Chemistry in the Upper Summer mesosphere, was a Swedish sounding rocket project led by MISU with contributions from Norway, Germany, Austria and the USA (Gumbel et al., 2013; Havnes et al., 2013; Hedin et al., 2013; Sternovsky et al., 2013). In this context, particle species comprise ice particles, smoke particles of meteoric origin, and possibly other background particles formed by conversion from trace gases. Important questions concerned both the properties of particle layers and their interaction with various phenomena in the mesosphere and lower thermosphere. This includes the relationship between smoke and ice, ice particle nucleation and evolution, and the possible influence of these particle species on chemistry. Both the German/Norwegian ECOMA project and PHOCUS aimed at the characterization of smoke and ice particles and their interactions. While ECOMA concentrated on interactions with ionospheric

processes, PHOCUS concentrated on interactions with neutral O_x/HO_x chemistry. The configuration of the front deck with the nosecone removed is shown in Fig. 18. The rocket measurements were complemented by ground-based instrumentation at Esrange (the ESRAD MST radar and the Esrange lidar), the EISCAT facility, the MORRO radar near Tromsø, and the MAARSY radar on Andøya.

One MAGIC sampler was prepared at Stockholm University with ultra thin carbon film on a holey carbon support film and 400 lines/inch Cu mesh. This time, only one grid was exposed in the altitude region were MSPs and ice particles are expected to be present. In addition, seven reference pins of two different types were prepared. Four pins were prepared in the same way as the exposed grid, i.e. a TEM grid with a Cu mask of 1 mm diameter aperture, while three pins were prepared with a Cu cap that completely covered the TEM grid (see Fig. 19). If the completely covered grids were to show particles after flight they would be contamination deposited on the grids in the clean room when mounting or removing the grids, or when being transferred to the TEM. As with the ECOMA 2008 campaign, a detailed characterization of the grids was made before flight (in the five squares as shown in Fig. 15a). No plasma cleaning was done this time. The characterization showed that these grids were very much cleaner compared to grids flown in earlier campaigns. The pre-flight EDX spectra of the grids showed C from the carbon film, Cu from the copper support mesh and a small Si signal from the detector itself, but no signal from the transition metals Cr, Mn, Fe or Ni that were seen earlier. A small amount of NaCl particles were seen which would be readily identified after flight as belonging to the grid from the beginning.

At the time of launch the Esrange lidar indicated the presence of a strong NLC layer and the Esrange MST radar, which had been monitoring the development of the PMSE during the morning hours, showed a narrowing and lowering of the PMSE layer indicating an aged ice layer with large particles. During flight the three on board NLC photometers detected a strong but thin NLC layer between 81 and 82 km altitude (Gumbel et al., 2013). The three different detectors for charged particles report a narrow structured layer between 81 and 82 km altitude (Havnes et al., 2013; Sternovsky et al., 2013). This does not mean that

there were no particles below or above this layer, but that they were too small to reach the detectors due to aerodynamics.

The TEM analysis after the flight showed no new particles on either of the two types of reference grids, i.e. no contamination of the grids occurred during handling or during flight. Detailed analysis of the exposed grid reveals no new particles either. This grid was exposed between 77.3 and 91 km altitude, i.e. from well below until high above the NLC ice particle layer at 81-82 km detected by the three charge impact detectors and the NLC photometers. Typical NLC particle number densities are around 100 cm^{-3} (e.g. von Cossart et al., 1999; Baumgarten et al., 2008) which means that, after passing through the 1 km NLC layer, there would be 0.1 ice particle impacts per square micrometre, or 160 impacts in each Cu grid square on the exposed TEM grid. The charged particle detectors estimate that there were one to two orders of magnitude more particles in the NLC layer, which means there would have been 1-10 particle impacts per square micrometre on the grid. The TEM investigations of the exposed grid show no evidence of particle impact or contamination (no sub-nanometre or nanometre sized particles, no holes in the C film, no monoliths or 25-200 nm radius particles, no ring-like structures or agglomerated particles) and no hydrocarbon contamination that were seen on earlier flights. Since particles were present in the altitude region sampled, as shown by the charge impact detectors, and must have impacted on the sampling grid, it must be concluded that the particles have bounced off and did not stick to the surface. For this flight it has thus been shown that no contamination was introduced during handling of the grids or during flight and that the sticking efficiencies for meteoric smoke and ice particles are most likely very small.

4. Summary and conclusion

The MAGIC meteoric smoke particle sampler was developed and built to allow for the first time MSPs to be sampled in the upper mesosphere and lower thermosphere and returned to the ground for detailed laboratory investigations. MAGIC samplers have been flown and successfully recovered on seven payloads. After all flights, except for PHOCUS, particles of different sizes, shapes and

composition were found. Particles of sizes and elemental composition similar to what can be expected for MSPs were found but due to challenges with large amounts of different types of contamination (particles and hydrocarbon film and drops) and large uncertainties in the sticking efficiency of the particles on the sampling surfaces, no conclusive results have been obtained. Table 3 summarises all successfully recovered flights and gives approximate sampling altitudes for each grid. The 2005 and 2006 launch campaigns were conducted during times when mesospheric ice particles were absent, i.e. outside polar summer conditions, while the 2008 and 2011 campaigns were conducted during peak NLC season with confirmed presence of ice particles. Models of the distribution of MSPs show that the particle concentration should be very much reduced in the polar summer mesosphere due to the general circulation of the atmosphere (e.g. Megner et al., 2008a). This would suggest that much more nanometre sized particles should be found on the grids from the non-summer flights compared to the summer flights. This is also what is seen, i.e. more particles on the grids from the non-summer flights. However, the amounts of particles on the non-summer flights are much too high (several orders of magnitude), even when a sticking efficiency of the particles on the carbon film of 100% is assumed, suggesting that a majority of them are contamination. The ECOMA-01 grids show heavy contamination from hydrocarbons and stainless steel particles and it is difficult to draw conclusions about possible other particles as they drown in the signal from the contamination. For the two summer campaigns no in-flight sampled nanometre sized particles were discovered on the grids. The ECOMA-05 and -06 grids were damaged during transport back to NRL, and particles found on the ECOMA-06 grids are most likely contamination. Analysis of the ECOMA-04 grids shows the presence of large spherical agglomerates (~0.5 – 0.8 μm radii) on the grid that was exposed during passage of the NLC layer, but also on the two reference grids (Figs 16 and 17). Such agglomerates have not been seen on any of the other flights of the MAGIC samplers, but show similarities to attempts to sample NLC particles in the 1960's. On the Wallops Island flight, holes in the ultra-thin C film (Fig. 10) and ring-like structures were seen (Fig. 11) that have not been seen on any of the other flights. Analysis of the PHOCUS grid shows no evidence of in-flight sampled particles of any size, neither on the exposed grid

nor on any of the reference grids. This suggests that the sticking efficiencies for both pure MSPs and MSPs contained in ice particles are very small. The lack of in-flight sampled nanometre sized particles on the summer flights also suggests that the improvements made to minimize the contamination had an effect and that the sampling process and handling of the samples has become cleaner.

As stressed earlier, the sticking efficiency for MSPs (pure and contained in ice particles) on the sampling surface is a major uncertainty. A recent study was made with C and Al_2O_3 particles impacting on surfaces of C, Au and grease (Reissaus et al., 2006). From this, a sticking efficiency for Al_2O_3 particles on C of ~14% was found (relative to a grease surface, for which a sticking efficiency of 100% for Al_2O_3 particles was assumed). The handling of such small particles is very difficult and the associated uncertainties of the properties of the impacting particles are large. It is also difficult to say how applicable this study is to actual rocket-borne sampling in the mesosphere. Studies have been made earlier on the capture and rebound of small particles upon impact with surfaces (e.g. Dahneke, 1971; Tsai et al., 1990), although at lower velocities, showing significant particle bounce.

The *in situ* sampling of MSPs remains an extremely challenging endeavour. Detailed studies are needed with different sampling surface types and a reliable source of MSP analogues under conditions relevant for mesospheric sampling from a sounding rocket (e.g. different velocities and angles of attack). Similar studies should be performed for dirty ice particles in the 30 to 100 nm radius size range. This is not only important for future instruments, but also to validate the MAGIC results. To collect as much MSPs as possible and keep the instrument simple, a single pin with a TEM grid should be exposed throughout the mesospheric dust layer, as was attempted on the PHOCUS payload. Then, after that successful sampling of MSPs has been demonstrated, the altitude distribution should be investigated. The rocket flight must be designed to maximize the probability of collecting MSPs. To minimize the risk of the particles bouncing off the surface, the apogee should be within the layer so that the sampling surface has a low relative velocity with respect to the dust and the payload should preferably be attitude controlled to maintain a small angle of attack. Different sampling surface materials should be investigated carefully. The

use of a soft material as the collection surface, such as e.g. aerogel, was considered at the early stages of the MAGIC design work. It was however felt at that time that the granularity of the aerogel was too coarse for the nanometre sized MSPs and that the preparation of such a sample for the TEM following a flight would introduce contaminants that would be difficult to distinguish from the MSPs. Therefore it was decided to use the cleaner solution of the TEM grids.

The MAGIC project was originally designed during a time when very little was known quantitatively on smoke particles in the mesosphere. Since then, major progress has been achieved by remote sensing (Hervig et al., 2009; 2012), rocket-borne measurements of charged particles (Rapp et al., 2010; 2012), radar studies (Strelnikova et al., 2007; Rapp et al., 2007), and numerical modelling (Megner et al., 2008b; Bardeen et al., 2008). Nevertheless, direct *in situ* sampling of MSPs is still highly desirable. Only direct *in situ* sampling can presumably provide final evidence about particle composition, size and shape. Knowledge about these microphysical properties continues to be a key to understanding both the evolution and the interaction of meteoric material in the mesosphere.

Acknowledgements*:* We acknowledge Robert R. Meier for the original idea to measure meteoric smoke particles. MAGIC was a NASA project funded under Grant No. NDPR S-06215-G. The MAGIC and PHOCUS sounding rocket projects were funded by the Swedish National Space Board. The ECOMA project was sponsored by the German Aerospace Center (DLR), and the Norwegian Space Center and the Research Council of Norway supported the Norwegian contribution. We thank for the opportunity to participate in the VTSRP and ECOMA projects with MAGIC MSP samplers, and acknowledge the excellent support of SSC, Esrange Space Center, Wallops Flight Facility, Andøya Rocket Range, the Norwegian Defence Research Establishment and DLR-Mobile Rocket Base (Moraba). The new electron microscopy facility at Stockholm University was made possible by the support from the Knut and Alice Wallenberg foundation.

References

Aikin, A. C., Grebowsky, J. M., and Burrows, J. P., 2004. Satellite measurements of

the atmospheric content of metallic ion and neutral species. Adv. Space Res., 33, 1481–1485.

Alpers, M., J. Höffner, J., and von Zahn, U., 1996. Upper-atmosphere Ca and Ca+ at midlatitudes—the first simultaneous and common-volume lidar observations. Geophys. Res. Lett., 23, 567–570.

Amyx, K., Sternovsky, Z., Knappmiller, S., Robertson, S., Horányi, M., and Gumbel, J., 2008. In-situ measurement of smoke particles in the wintertime polar mesosphere between 80 and 85 km altitude. J. Atmos. Sol.-Terr. Phys., 70, 61–70.

Bardeen, C. G., Toon, O. B., Jensen, E. J., Marsh, D. R., and Harvey, V. L., 2008. Numerical simulations of the three dimensional distribution of meteoric dust in the mesosphere and upper stratosphere. J. Geophys. Res., 113, D17202, doi:10.1029/2007JD009515.

Barjatya, A. and Swenson, C. M., 2006. Observations of triboelectric charging effects on Langmuir-type probes in dusty plasma. J. Geophys. Res., 111, A10302, doi:10.1029/2006JA011806.

Baumgarten, G., Fiedler, J., Lübken, F.-J., and von Cossart, G., 2008. Particle properties and water content of noctilucent clouds and their interannual variation. J. Geophys. Res., 13, D06203, doi:10.1029/2007JD008884.

Bowman, M.R., Gibson, A.J., Sandford, M.C., 1969. Atmospheric sodium measured by a tuned laser radar. Nature 221, 456–458.

Ceplecha, Z., Borovicka, J., Elford, W. G., ReVelle, D. O., Hawkes, R. L., Porubcan, V., and Simek, M., 1998. Meteor phenomena and bodies. Space Sci. Rev., 84, 327–471.

Chamberlain, J.W., Hunten, D.M., Mack, J.E., 1958. Resonance scattering by atmospheric sodium-IV abundance of sodium in twilight. J. Atmos. Terr. Phys. 12, 153–165.

Conway, R. R., Summers, M. E., Stevens, M. H., Cardon, J. G., Preusse, P., and Offermann, D., 2000. Satellite observations of upper stratospheric and mesospheric OH: The HOx dilemma. Geophys. Res. Lett., 27, 2613-2616.

Croskey, C., Mitchell, J., Friedrich, M., Torkar, K., Hoppe, U.-P., and Goldberg, R., 2001. Electrical structure of PMSE and NLC regions during the DROPPS program. Geophys. Res. Lett., 28, 1427– 1430.

Curtius, J., Weigel, R., Vössing, H.-J., Wernli, H., Werner, A., Volk, C.-M., Konopka, P., Krebsbach, M., Schiller, C., Roiger, A., Schlager, H., Dreiling, V., and Borrmann, S., 2005. Observations of meteoric material and implications for aerosol nucleation in the winter Arctic lower stratosphere derived from in situ particle measurements. Atmos. Chem. Phys., 5, 3053-3069.

Cziczo, D. J., Thomson, D. S., and Murphy, D. M., 2001. Ablation, flux, and atmospheric implications of meteors inferred from stratospheric aerosol. Science, 291, 1772-1775.

Dahneke, B., 1971. The Capture of Aerosol Particles by Surfaces. J. Coll. Int. Sci., 37, 2, 342-353.

Dhomse, S. S., Saunders, R. W., Tian, W., Chipperfield, M. P., and Plane, J. M. C., 2013. Plutonium-238 observations as a test of modeled transport and surface deposition of meteoric smoke particles. Geophys. Res. Lett., 40, 4454–4458, doi:10.1002/grl.50840.

Donahue, T.M., Meier, R.R., 1967. Distribution of sodium in daytime upper atmosphere as measured by a rocket experiment. J. Geophys. Res., 72, 2803–2821.

Donahue, T.M., Guenther, B., Blamont, J.E., 1972. Noctilucent clouds in daytime: circumpolar particulate layers near the summer mesopause. J. Atmos. Sci. 29, 1205–1209.

Eska, V., Höffner, J., and von Zahn, U., 1998. Upper atmosphere potassium layer and its seasonal variations at 54°N. J. Geophys. Res., 103, 29207–29214.

Farlow, N. H., Ferry, G. V., and Blanchard, M. B., 1970. Examination of Surfaces Exposed to a Noctilucent Cloud, August 1, 1968. J. Geophys. Res., 75, 33, 6736-6750.

Fentzke, J. T., Janches, D., Strelnikova, I., and Rapp, M., 2009. Meteoric smoke particles derived using dual beam Arecibo UHF observations of D-region spectra during different seasons. J. Atmos. Sol.-Terr. Phys., 71, 1982–1991, doi:10.1016/j.jastp.2009.09.002.

Friedrich, M., Rapp, M., Plane, J. M. C., and Torkar, K. M., 2011. Bite-outs and other depletions of mesospheric electrons. J. Atmos. Sol.-Terr. Phys., 73, 2201–2211, doi:10.1016/j.jastp.2010.10.018.

Fussen, D., Vanhellemont, F., Tétard, C., Mateshvili, N., Dekemper, E., Loodts, N., Bingen, C., Kyrölä, E., Tamminen, J., Sofieva, V., Hauchecorne, A., Dalaudier, F., Bertaux, J.-L., Barrot, G., Blanot, L., Fantond'Andon, O., Fehr, T., Saavedra, L., Yuan, T., She, C.-Y., 2010. A global climatology of the mesospheric sodium layer from GOMOS data during the 2002–2008 period. Atmos. Chem. Phys., 10, 9225-9236.

Gabrielli, P., Barbante, C., Plane, J. M. C., Varga, A., Hong, S., Cozzi, G., Gaspari, V., Planchon, F. A. M., Cairns, W., Ferrari, C., Crutzen, P., Cescon, P., and Boutron, C. F., 2004. Meteoric smoke fallout over the Holocence epoch revealed by iridium and platinum in Greenland ice. Nature, 432, 1011–1014, doi:10.1038/nature03137.

Gadsden, M., and Schröder, W. 1989. Noctilucent Clouds. Physics and chemistry in space 18, Springer-Verlag.

Gelinas, L. J., Lynch, K. A., Kelley, M. C., Collins, R. L., Baker, S., Zhou, Q., and Friedman, J. S., 1998. First observation of meteoritic charged dust in the tropical mesosphere. Geophys. Res. Lett., 25, 4047–4050.

Gumbel, J., 2001. Aerodynamic influences on atmospheric in situ measurements from sounding rockets. J. Geophys. Res., 106, 10553-10563.

Gumbel, J., and Megner, L., 2009. Charged meteoric smoke as ice nuclei in the mesosphere: Part 1 - A review of basic concepts. J. Atmos. Sol.-Terr. Phys., 71, 1225–1235.

Gumbel, J., Murtagh, D. P., Witt, G., Espy, P. J., and Schmidlin, F. J., 1998. Odd oxygen measurements during the NLC-93 rocket campaign. J. Geophys. Res., 103, 23399-23414.

Gumbel, J., Waldemarsson, T., Giovane F., Khaplanov, M., Hedin J., Karlsson B., Lossow, S., Megner L., Stegman J., Fricke, K. H., Blum, U., Voelger P., Kirkwood, S., Dalin. P. Sternovsky, Z., Robertson S., Horányi, M., Stroud, R., Siskind, D. E., Meier, R. R., Blum, J., Summers, M., Plane, J. M. C., Mitchell N. J., and Rapp, M., 2005. The MAGIC rocket campaign – an overview. Proc. 17th ESA Symposium on European Rocket and Balloon Programmes and Related Research (ESA SP-590), 141–144.

Gumbel, J., et al., 2013. The PHOCUS Campaign. J. Atmos. Sol.-Terr. Phys., (this issue)

Havnes, O., and Næsheim, L. I., 2007. On the secondary charging effects and structure of mesospheric dust particles impacting on rocket probes. Ann. Geophys., 25, 623–637.

Havnes, O., Trøim, J., Blix, T., Mortensen, W., Næsheim, L. I., Thrane, E., and Tønnesen, T., 1996. First detection of charged dust particles in the Earth's mesosphere. J. Geophys. Res., 101, 10 839–10 847.

Havnes, O., Gumbel, J., La Hoz, C., and Hedin, J., 2013. On the size distribution of collision fragments of NLC dust particles and their relevance to meteoric smoke particles. J. Atmos. Sol.-Terr. Phys., (this issue)

Hedin, J., and Gumbel, J., 2011. The global mesospheric sodium layer observed by Odin/OSIRIS in 2004–2009. J. Atmos. Sol.-Terr. Phys., 73, 2221–2227.

Hedin, J., Gumbel, J., Rapp, M., 2007a. On the efficiency of rocket-borne detection in the mesosphere. Atmos. Chem. Phys. 7, 3701–3711.

Hedin, J., Gumbel, J., Waldemarsson, T., and Giovane, F., 2007b. The aerodynamics of the MAGIC meteoric smoke sampler. Adv. Space Res., 40, 6, 818-824, doi:10.1016/j.asr.2007.06.046.

Hedin, J., Gumbel, J., Khaplanov, M., Stegman, J., Witt, G., and Murtagh, D. P., 2013. Chemical composition from rocket-borne O2($a^1\Delta_g$) airglow photometry during PHOCUS. J. Atmos. Sol.-Terr. Phys., (this issue).

Hemenway, C. L., Soberman, R. K., and Witt, G., 1964a. Sampling of noctilucent cloud particles. Tellus XVI, 1, 84-88.

Hemenway, C. L., Fullam, E. F., Skrivanek, R. A., Soberman, R. K., and Witt, G., 1964b. Electron microscope studies of noctilucent cloud particles. Tellus, XVI, 1, 96-102.

Hervig, M. E., Thompson, R. E., McHugh, M., Gordley, L. L., Russell III, J. M., and Summers, M. E., 2001. First confirmation that water ice is the primary component of polar mesospheric clouds. Geophys. Res. Lett., 28, 971-974.

Hervig, M. E., Gordley, L. L., Deaver, L. E., Siskind, D. E., Stevens, M. H., Russell III, J. M., Bailey, S. M., Megner, L., and Bardeen, C. G., 2009. First satellite observations of meteoric smoke in the upper atmosphere. Geophys. Res. Lett., 113, L18805, doi:10.1029/2009GL039737.

Hervig, M. E., Deaver, L. E., Bardeen, C. G., Russell III, J. M., Bailey, S. M., and Gordley, L. L., 2012. The content and composition of meteoric smoke in mesospheric ice particles from SOFIE observations. J. Atmos. Sol.-Terr. Phys., 84–85, 1–6.

Horányi, M., Gumbel, J., Witt, G., and Robertson, S., 1999. Simulation of rocket-borne particle measurements in the mesosphere. Geophys. Res. Lett., 26, 1537-1540.

Horányi, M., Robertson, S., Smiley, B., Gumbel, J., Witt, G., and Walch, B., 2000. Rocket-borne mesospheric measurement of heavy (m $\gg$ 10 amu) charge carriers. Geophysical Research Letters, 27, 3825–3828.

Hughes, D. W., 1978. Meteors, in Cosmic Dust (ed. McDonnel, J. A. M.), Wiley, Chichester.

Hunten, D. M., Turco, R. P., and Toon, O. B., 1980. Smoke and dust particles of meteoric origin in the mesosphere and thermosphere. J. Atmos. Sci., 37, 1342—1357.

Kalashnikova, O., Horányi, M., Thomas, G. E., and Toon, O. B., 2000. Meteoric smoke production in the atmosphere. Geophys. Res. Lett., 27, 3293-3296.

Kassa, M., Rapp, M., Hartquist, T.W., Havnes, O., 2012. Secondary charging effects due to icy dust particle impacts on rocket payloads. Ann. Geophys., 30, 433–439, doi:10.5194/angeo-30-433-2012.

Khaplanov M., Gumbel, J., Wilhelm, N., and Witt, G., 1996. Hygrosonde – A direct measurement of water vapor in the stratosphere and mesosphere. Geophys. Res. Lett., 23 (13), 1645-1648.

Kopp, E., 1997. On the abundance of metal ions in the lower ionosphere, J. Geophys. Res., 102, 9667–9674.

Lanci, L. and Kent, D. V., 2006. Meteoric smoke fallout revealed by superparamagnetism in Greenland ice. Geophys. Res. Lett., 33, L13308, doi:10.1029/2006GL026480.

Latteck, R , Singer, W., Rapp, M., Vandepeer, B., Renkwitz, T., Zecha, M., and Stober, G., 2012. MAARSY: The new MST radar on Andoya-System description and first results. Radio Science, 47, RS1006, doi: 10.1029/2011RS004775

Lossow S., Khaplanov, M., Gumbel, J., Stegman, J., Witt, G., Dalin, P., Kirkwood, S., Schmidlin, F. J., Fricke, K. H., and Blum, U. A., 2008. Middle atmospheric water vapour and dynamics in the vicinity of the polar vortex during the Hygrosonde-2 campaign, Atmos. Chem. Phys. Disc., 8, 12227-12252.

Love, S. G. and Brownlee, D. E., 1993. A direct measurement of the terrestrial mass accretion rate of cosmic dust. Science, 262, 550– 553.

Lynch, K. A., Gelinas, L. J., Kelley, M. C., Collins, R. L., Widholm, M., Rau, D., MacDonald, E., Liu, Y., Ulwick, J., and Mace, P., 2005. Multiple sounding rocket observations of charged dust in the polar winter mesosphere. J. Geophys. Res., 110, A03302, doi:10.1029/2004JA010502.

Mathews, J. D., Janches, D., Meisel, D. D., and Zhou, Q. H., 2001. The micrometeroid mass flux into the upper atmosphere: Arecibo results and a comparison with prior estimates, Geophys. Res. Lett., 28, 1929–1932.

McNeil, W. J., Lai, S. T., and Murad, E., 1998. Differential ablation of cosmic dust and implications for the relative abundances of atmospheric metals. J. Geophys. Res., 103, 10899-10911, doi:10.1029/98JD00282.

Megner, L., 2007. Funneling of Meteoric Material into the Polar Winter Vortex, Proc. 17th Int. Conf. on Nucleation and Atmospheric Aerosols, Galway, O'Dowd, G.D. and Wagner, P.E., Eds., pp. 860–864.

Megner, L., and Gumbel, J., 2009. Charged meteoric particles as ice nuclei in the mesosphere: Part 2 - A feasibility study. J. Atmos. Sol.-Terr. Phys., 71, 1236–1244.

Megner, L., Rapp, M., and Gumbel, J., 2006. Distribution of meteoric smoke – sensitivity to microphysical properties and atmospheric conditions, Atmos. Chem. Phys., 6, 4415–4426.

Megner, L., Gumbel, J., Rapp, M. and Siskind, D. E., 2008a. Reduced meteoric smoke particle density at the summer pole–Implications for mesospheric ice particle nucleation. Adv. Space Res., 41, 1, 41–49, doi:10.1016/j.asr.2007.09.006.

Megner, L., Siskind, D. E., Rapp, M., and Gumbel, J., 2008b. Global and temporal distribution of meteoric smoke: A two- dimensional simulation study, J. Geophys. Res., 113, D03202, doi:10.1029/2007JD009054.

Murad, E., Swider, W., and Benson, S., W., 1981. Possible role of metals in stratospheric chlorine chemistry. Nature, 289, 273-274.

Murphy, D., Thomson, D., and Mahoney, M., 1998. In Situ Measurements of Organics, Meteoritic Material, Mercury, and Other Elements in Aerosols at 5 to 19 Kilometers. Science, 282(5394), 1664, doi:10.1126/science.282.5394.1664.

Newman, A.L., 1988. Nighttime Na D emission observed from a polar orbiting DMSP satellite. J. Geophys. Res. 93, 4067–4075.

Plane, J. M. C., 2003. Atmospheric chemistry of meteoric metals. Chem. Rev., 103, 12, 4963–4984, doi:10.1021/cr0205309.

Plane, J. M. C., 2004. A time-resolved model of the mesospheric Na layer: constraints on the meteor input function. Atmos. Chem. Phys., 4, 627-638.

Plane, J. M. C., 2012. Cosmic dust in the earth's atmosphere. Chem. Soc. Rev., 41, 6507–6518.

Plane, J. M. C. and Whalley, C. L., 2012. A new model for magnesium chemistry in the upper atmosphere. J. Phys. Chem. A, 116, 6240– 6252.

Rapp, M., 2009. Charging of mesospheric aerosol particles: the role of photodetachment and photoionization from meteoric smoke and ice particles. Ann. Geophys., 27, 2417–2422, doi:10.5194/angeo-27-2417-2009.

Rapp, M. and Lübken, F.-J., 2001. Modelling of particle charging in the polar summer mesosphere: part 1 – general results. J. Atmos. Sol.-Terr. Phys., 63, 759–770.

Rapp, M., and Lübken, F.-J. 2004. Polar mesosphere summer echoes (PMSE): Review of observations and current understanding, Atmos. Chem. Phys., 4, 2601–2633.

Rapp, M., and Strelnikova, I., 2009. Measurements of meteor smoke particles during the ECOMA-2006 campaign: 1. Particle detection by active photoionization. J. Atmos. Sol. Terr. Phys., 71, 477–485.

Rapp, M. and Thomas, G. E., 2006. Modeling the microphysics of mesospheric ice particles – assessment of current capabilities and basic sensitivities. J. Atmos. Sol.-Terr. Phys., 68, 715–744.

Rapp, M., Hedin, J., Strelnikova, I., Friedrich, M., Gumbel, J., and Lübken, F.-J., 2005. Observations of positively charged nanoparticles in the nighttime polar mesosphere. Geophys. Res. Lett., 32, L23821, doi:10.1029/2005GL024676

Rapp, M., Strelnikova, I., and Gumbel, J., 2007. Meteoric smoke particles: evidence from rocket and radar techniques. Adv. Space Res., 40, 809–817, doi:10.1016/j.asr.2006.11.021.

Rapp, M., Strelnikova, I., Strelnikov, B., Hoffmann, P., Friedrich, M., Gumbel, J., Megner, L., Hoppe, U.-P., Robertson, S., Knappmiller, S., Wolff, M., and Marsh, D. R., 2010. Rocket-borne in-situ measurements of meteor smoke: charging properties and implications for seasonal variation. J. Geophys. Res., 115, D00I16, doi:10.1029/2009JD012725.

Rapp, M., Plane, J. M. C., Strelnikov, B., Stober, G., Ernst, S., Hedin, J., Friedrich, M., and Hoppe, U.-P., 2012. In situ observations of meteor smoke particles (MSP) during the Geminids 2010: constraints on MSP size, work function and composition. Ann. Geophys., 30, 1661–1673, doi:10.5194/angeo-30-1661-2012.

Reid, W., Achtert, P., Ivchenko, N., Magnusson, P., Kuremyr, T., Shepenkov, V., and Tibert, G., 2013. Technical Note: A novel rocket-based in situ collection technique for mesospheric and stratospheric aerosol particles. Atmos. Meas. Tech., 6, 777–785, doi:10.5194/amt-6-777-2013.

Reissaus, P., Waldemarsson, T., Blum, J., Clément, D., Llamas, I., Mutschke, H., and Giovane, F., 2006. Sticking efficiency of nanoparticles in high-velocity collisions with various target materials. J. Nanopart. Res., 8, 693–703, doi:10.1007/s11051-006-9102-9.

Robertson, S., Smiley, B., Sternovsky, Z., Gumbel, J., and Stegman, J., 2004. Rocket-borne probes for charged ionospheric aerosol particles. IEEE Trans. Plasma Sci., 32, 716–723.

Robertson, S., Horányi, M., Knappmiller, S., Sternovsky, Z., Holzworth, R., Shimogawa, M., Friedrich, M., Torkar, K., Gumbel, J., Megner, L., Baumgarten, G., Latteck, R., Rapp, M., Hoppe, U.-P., and Hervig, M. R., 2009. Mass analysis of charged aerosol particles in NLC and PMSE during the ECOMA/MASS campaign, Ann. Geophys., 27, 1213–1232.

Robertson, S., Dickson, S., Horányi, M., Sternovsky, Z., Friedrich, M., Janches, D., Megner, L., and Williams, B., 2013. Detection of Meteoric Smoke Particles in the Mesosphere by a Rocket-borne Mass Spectrometer. J. Atmos. Sol.-Terr. Phys., (this issue) http://dx.doi.org/10.1016/j.jastp.2013.07.007.

Rosinski, J., and Snow, R. H., 1961. Secondary particulate matter from meteor vapors. J. Meteorol., 18, 736–745.

Saunders, R. W., and Plane, J. M. C., 2006. A laboratory study of meteor smoke analogues: Composition, optical properties and growth kinetics. J. Atmos. Sol.-Terr. Phys., 68, 2182–2202.

Saunders, R. W., and Plane, J. M. C., 2011. A Photo-Chemical Method for the Production of Olivine Nanoparticles as Cosmic Dust Analogues. Icarus 212, 373-382.

Saunders, R. W., Dhomse, S., Tian, W. S., Chipperfield, M. P., and Plane, J. M. C., 2012. Interactions of meteoric smoke particles with sulphuric acid in the Earth's stratosphere. Atmos. Chem. Phys., 12, 4387–4398.

Schulte, P., and Arnold, F., 1992. Detection of upper atmospheric negatively charged microclusters by a rocket borne mass spectrometer. Geophys. Res. Lett., 19, 2297–2300.

Self, D. E., and Plane, J. M. C., 2003. A kinetic study of the reactions of iron oxides and hydroxides relevant to the chemistry of iron in the upper atmosphere. Phys. Chem. Chem. Phys., 5, 1407–1418.

Skrivanek, R. A., and Soberman, R. K., 1964. Simulation of ring patterns observed with noctilucent cloud particles. Tellus, XVI, 1, 114-117.

Smiley, B., Rapp, M., Blix, T. A., Robertson, S., Horányi, M., Latteck, R., and Fiedler, J., 2006. Charge and size distribution of mesospheric aerosol particles measured inside NLC and PMSE during MIDAS MaCWAVE 2002. J. Atmos. Sol.-Terr. Phys., 68, 114– 123.

Soberman, R. K., and Hemenway, C. L., 1965. Meteoric Dust in the Upper Atmosphere. J. Geophys. Res., 70, 19, 4943-4949.

Sternovsky, Z., Robertson, S., Dickson, S., Gumbel, J., Hedin, J., Strelnikov, B., Asmus, H., and Havnes, O., 2013. In-situ Detection of Noctilucent Cloud Particles by the Colorado Dust Detectors onboard the PHOCUS Campaign. J. Atmos. Sol.-Terr. Phys., (this issue), http://dx.doi.org/10.1016/j.jastp.2014.01.018.

Strelnikova, I., Rapp, M., Raizada, S., and Sulzer, M., 2007. Meteor smoke particle properties derived from Arecibo incoherent scatter radar observations. Geophys. Res. Lett., 34, L15815, doi:10.1029/2007GL030635.

Strelnikova, I., Rapp, M., Strelnikov, B., Baumgarten, G., Brattli, A., Svenes, K., Hoppe, U.-P., Friedrich, M., Gumbel, J., and Williams, B., 2009. Measurements of meteor smoke particles during the ECOMA-2006 campaign: 2. Results. J. Atmos. Sol. Terr. Phys., 71, 486–496.

Summers M. E. and Siskind, D. E., 1999. Surface recombination of O and H_2 on meteoric dust as a source of mesospheric water vapor. Geophys. Res. Lett., 26, 1837–1840.

Thomas, G. E., 1991. Mesospheric clouds and the physics of the mesopause region. Rev. Geophys., 29, 553-575.

Tsai, C.-J., Pui, D. Y. H., and Liu, B. Y. H., 1990. Capture and Rebound of Small Particles Upon Impact with Solid Surfaces. Aerosol Sci. Tech., 12, 497-507.

Voigt, C., Schlager, H., Luo, B. P., Dörnbrack, A. Roiger, A., Stock, P., Curtius, J., Vössing, H., Borrmann, S., Davies, S., Konopka, P., Schiller, C., Shur, G., and Peter, T., 2005. Nitric acid trihydrate (NAT) formation at low NAT supersaturation in polar stratospheric clouds (PSCs). Atmos. Chem. Phys, 5, 1371–1380.

von Cossart, G., Fiedler, J., and von Zahn, U., 1999. Size distribution of NLC particles as determined from 3-color observations of NLC by ground-based lidar. Geophys. Res. Lett., 26 (11), 1513-1516.

von Zahn, U., 2005. The total mass flux of meteoroids into the Earth's upper atmosphere. Proc. 17th ESA Symposium on European Rocket and Balloon Programmes and Related Research (ESA SP-590), 33–39.

Vondrak, T., Plane, J.M.C., Broadley, S., Janches, D., 2008. A chemical model of meteoric ablation. Atmos. Chem. Phys. 8 (23), 7015-7031.

Zeller, O., Zecha,M., Bremer, J., Latteck, R., and Singer, W. 2006. Mean characteristics of mesosphere winter echoes at mid- and high-latitudes, J. Atmos. Sol. Terr. Phys., 68 (10), 1087– 1104.

Figure captions

Figure 1. Simulated particle trajectories of (a) 0.4, (b) 0.6 and (c) 0.8 nm radius particles around the MAGIC sampling surface at 80 km altitude (from Hedin et al., 2007b). The grey scale is the air number density normalized to the unperturbed free-stream conditions.

Figure 2. The effective relative cross section of the MAGIC sampling surface for (a) various particle sizes as a function of altitude and (b) various altitudes as a function of particle size (from Hedin et al., 2007b).

Figure 3. (a) Instrument sketch of the collection mechanism inside the MAGIC instrument. **(b)** Close-up photo of the revolver with 9 collection pins. **(c)** The MAGIC collector unit with extended sampling pin. The cylindrical section houses the revolver with eight collection pins and one reference pin. The lower rectangular section houses the collection and extension mechanism. The included 50 cm scale indicates the size of the MAGIC instrument. **(d)** Close-up photo of the 3 mm diameter TEM grid mounted with Cu cap on top of an extended sampling pin.

Figure 4. The top of the MAGIC sounding rocket payload launched from Esrange in January 2005. A sampling pin is extended from one of the three MAGIC sampling units surrounding the Hygrosonde instrument (Khaplanov et al., 1996; Lossow et al, 2008a) in the centre.

Figure 5. a) The centre of the 30 nm thick continuous carbon film (grey) on 200 lines/ inch copper mesh (black) TEM grid used in the Esrange flight. b) Centre of the 3 nm ultra thin carbon film (light grey) on holey carbon film (or carbon mesh, dark grey net) and 400 lines/inch copper mesh (black) TEM grid used in the Wallops Island flight.

Figure 6. A MAGIC sampling pin extended through the forward bulkhead in front of the VTSRP payload launched at Wallops Island in 2005.

Figure 7. a) High-resolution bright-field TEM image of the grid exposed between 93.3 and 94.5 km, while **b)** is a high-angle annular dark-field (HAADF) image of that same area, showing particles in the 1-5 nm radius size range. Panels **c)** and **d)** are HAADF images of the collection grid exposed between 86.3 and 89.3 km showing particles in the 2-10 nm radius size range. The square patterns show the effect of the thin film of hydrocarbon present on the grid. Panel **e)** shows a large particle from the grid exposed between 90.3 and 94.3 km containing Ti, Si, Na, K, Ca, and Al and panel **f)** shows a particle with similar composition and morphology found on one of the unexposed reference grids. Panel **g)** shows a particle found on the grid exposed between 93.3 and 94.5 km and contain Fe, Si Al, Ca and Cr, while panel **h)** show a particle of similar composition and morphology found on one of the reference grids.

Figure 8. Measurement of mesospheric particles by the Colorado dust detectors (CDDs) on board the MAGIC sounding rocket (Amyx et al., 2008). The vertical lines indicate where MAGIC detectors sampled the atmosphere in the altitude range where the CDDs indicated presence of particles (e.g. M1G3 indicates grid 3 on MAGIC sampler 1 and M3G4 indicates grid 4 on MAGIC sampler 3 etc.).

Figure 9. High-angle annular dark-field (HAADF) image of atmospheric nanoparticles. The colour values in the image represent scattering intensity, which is a function of material thickness and composition. The yellow area is a 30 nm thick region of the supporting holey carbon collection film; the red areas are particles 0.5 to 2 nm in radius; and the blue areas are bare regions of the 3 nm ultra thin portions of collection film. The particles form what appears to be a fractal aggregate, which varies in density. The large red spot is a densely packed region of the 0.5 to 2 nm particles.

Figure 10. High-angle annular dark-field (HAADF) image of representative particle morphologies. As in Fig. 9, the 30 nm thick holey carbon support mesh appears yellow, and bare regions of the ultra thin 3 nm carbon film are blue. Particles range from red to yellow in appearance, depending on thickness and

compositions. Particle clusters are distributed across the film. The two angle brackets define a region of reduced intensity where prior observation at higher magnification resulted in the loss of an unknown sub-nm material that is readily vaporized under the electron beam. The vertical arrows indicate holes in the film, rimmed with concentrated material. The diagonal arrow indicates a particle ring, which appears to result from the concentration of particles around the perimeter of an evaporated liquid droplet.

Figure 11. High-angle annular dark-field (HAADF) image of a particle ring. The ring has a diffuse boundary of concentrated sub-nm material and is studded with dense aggregates of 0.5 to 2 nm radius particles.

Figure 12. a) The top section of the ECOMA payload for mesospheric particle studies with booms deployed. The ECOMA particle detector from IAP is in the centre and the MAGIC particle sampler from MISU/NRL in the foreground. Other instruments are temperature probes from IAP (left, right) and ionospheric instrumentation from the Technical University Graz, Austria (booms). **b)** Top section with the two MAGIC samplers visible and one half of the nosecone attached. For the 2008 campaign one MAGIC sampler was replaced by a mass dummy, and the two IAP temperature probes were replaced by the particle detectors from University of Tromsø, Norway and Dartmouth College, USA. **c)** Photo showing the extension added in the ECOMA 2007 and 2008 campaigns to protect the MAGIC pin exit hole and the volume around it from the possible airflow through the ECOMA detector and from the high temperatures during re-entry.

Figure 13. The different kinds of hydrocarbon contamination seen on the TEM grids in MAGIC sampler #1 on ECOMA-01. Low resolution TEM image showing **a)** lighter, irregularly shaped hydrocarbon blobs with central dark spot on grid 1, and **b)** darker, opaque, roundish hydrocarbon blobs on grid 7. **c)** Higher resolution HAADF image showing “snow flake” type hydrocarbon contamination on grid 2 with large amounts of nanometre sized particles with composition typical to stainless steel.

Figure 14. High-angle annular dark-field (HAADF) images of areas on ECOMA-01 grids 1, 2, 3 and 7 exposed to the atmosphere at 68.4-73.2 km, 78.1-86.2 km, 88.9-92.7 km, and 111.0-115.8 km altitude, respectively. Grids 2 and 3 show at least one order of magnitude more sub-10 nm particles per unit area than grids 1 and 7. EDX spectra show that the particles have a composition similar to stainless steel.

Figure 15. (a) Sketch of the TEM grid with aperture showing the 4 sampling squares in the centre and the on-grid reference square under the Cu mask, that was analysed both before and after flight. (b) Sketch of the sampling head on the collection pin with Cu mask, or grid aperture (grid apertures were not used for the two flights in 2005). (c) Photo of the copper grid cap, Cu mask (grid aperture), TEM grid, and the fully assembled sampling pin.

Figure 16. a) TEM image of an agglomerated particle found on the grid exposed to the NLC during the flight of ECOMA-04 from Andøya Rocket Range in June 2008. Panels **b)** to **n)** are energy-filtered images showing the signal from **b)** S, **c)** O, **d)** Na, **e)** Cu, **f)** Si, **g)** Mn, **h)** Mg, **i)** F, **j)** Cr, **k)** K, **l)** Fe, **m)** Cl, and **n)** Ca.

Figure 17. TEM images of agglomerated particles found **a)** on the on-grid reference square under the mask on the grid exposed to the NLC, and **b)** and **c)** on the reference grid that was not exposed to the atmosphere.

Figure 18. The top deck configuration of the PHOCUS sounding rocket payload launched from Esrange Space Center in July 2011 with the MAGIC particle sampler circled. Other instruments are the positive ion probe, electron probe, and the Faraday rotation experiment (the four booms, Technical University Graz); the IR airglow photometers and NLC photometers (the four black cylinders, MISU); the two detectors for charged particles (University of Tromsø (right) and IAP (left)); and the forward-looking water vapour radiometer in the centre (Chalmers University of Technology).

Figure 19. The two types of sampling pins prepared for the PHOCUS sounding rocket. Panel **a)** shows the normal open type used for four of the reference grids and the exposed grid, and **b)** shows the covered type used for three reference grids where the TEM grid is completely covered by a Cu cap.

Table 1. ECOMA-04 composition analysis before and after flight. Numbers given are the atomic %. The colour code is as follows: white marks signals below the detection limit both before and after flight; green marks elements that did not change; blue marks elements that were reduced after flight; and red marks elements that were increased after flight. The red squares mark the elements where there was a significant change.

	Grid 1	Grid 2	Grid 3	Grid 4	Grid 5 (ref)	Grid 6 (ref)
Element	**Before - After**	**Before - After**	**Before - After**	**Before - After**	**Before - After**	**Before - After**
C	96.0 – 96.0	96.5 – 96.2	95.4 – 95.9	96.0 – 95.7	95.8 – 92.3	96.0 – 96.6
O	3.5 – 3.5	2.5 – 2.4	4.0 – 2.4	3.4 – 2.8	3.4 – 2.2	3.5 – 0.78
F	0.5 – 0.3	0.06 – 0.03	0.03 – 0.05	0.05 – 0.15	0.07 – 3.6	0.15 – 0.05
Na	<0.01 -<0.01	0.01 -<0.01	<0.01 - 0.02	<0.01 -<0.01	<0.01 -0.02	N.A. - 0.04
Mg	<0.01 - <0.01	0.01 - 0.02	<0.01 - <0.01	<0.01 - <0.01	<0.01 - <0.01	N.A. - <0.01
Al	0.01 - <0.01	0.05 - <0.01	<0.01 - <0.01	<0.01 - <0.01	<0.01 - <0.01	0.01 - <0.01
Si	0.02 - 0.02	0.04 - <0.01	0.03 - 0.07	0.02 - 0.02	0.01 - <0.01	0.03 - 0.04
S	<0.01 - <0.01	<0.01 - <0.01	<0.01 - <0.01	<0.01 - <0.01	<0.01 - 0.01	0.03 - <0.01
Cl	<0.01 - <0.01	<0.01 - <0.01	<0.01 - <0.01	<0.01 - <0.01	<0.01 - <0.01	N.A. - 0.01
K	<0.01 - <0.01	<0.01 - <0.01	<0.01 - <0.01	<0.01 - 0.01	<0.01 - <0.01	<0.01 - <0.01
Ca	<0.01 - <0.01	<0.01 - <0.01	<0.01 - <0.01	<0.01 - <0.01	<0.01 - <0.01	N.A. - <0.01
Ti	<0.01 - <0.01	<0.01 - <0.01	<0.01 - <0.01	<0.01 - <0.01	<0.01 - <0.01	N.A. - <0.01
Cr	0.01 - 0.02	<0.01 - 0.01	0.01 - <0.01	0.01 - 0.01	0.01 - <0.01	0.01 - <0.01
Mn	0.02 - 0.02	<0.01 - <0.01	<0.01 - <0.01	0.01 - 0.01	0.02 - <0.01	<0.01 - <0.01
Fe	0.01 - 0.02	<0.01 - <0.01	0.02 - <0.01	0.02 - 0.03	0.02 - <0.01	0.05 - 0.01
Ni	<0.01 - <0.01	<0.01 - 0.01	<0.01 - 0.01	<0.01 - <0.01	<0.01 - 0.01	N.A. - <0.01
Cu	0.35 - 0.70	0.80 -1.31	0.48 - 1.50	0.48 – 1.24	0.64 - 1.63	0.60 - 2.33

Table 2. The amount of particles found on the ECOMA-06 MAGIC grids. The mesospheric particle density is calculated assuming a sticking efficiency of 100 %. The numbers in parenthesis after the mean radius are the minimum and maximum radii (or spread) of the measured particle size distribution.

Grid	Particles on grid (μm^{-2})	Mean radius (nm)	Sampled altitude (km)	Particle density (cm^{-3})
1	76.3	4.51 (2.5 - 9)	65.5 – 70 (4.5 km)	1.7×10^{4}
2	13.0	4.51 (2.5 - 9.8)	75 – 87 (12 km)	1.1×10^{3}
3	23.2	4.93 (3.3 - 9.8)	90 – 94 (4 km)	5.8×10^{3}
4	14.5	4.13 (2.5 - 9.8)	96.5 – 100.5 (4 km)	3.6×10^{3}
5	11.0	4.55 (2.5 - 12.7)	Reference	-
6	31.4	4.13 (2-12.7)	Reference	-

Table 3. Summary of all successfully recovered MAGIC flights.

Campaign	MAGIC Campaign 2005			VTSRP	ECOMA Campaign in 2006 & 2008					PHOCUS
	M-1	M-2	M-3	2005	E01-1	E01-2	E04	E05	E06	2011
Time	10 January -05 04:37 UT			17 May-05	8 September -06 22:17 UT		30 June-08 13:22 UT	7 July-08 21:24 UT	12 July-08 10:46 UT	21 Jul-11 07:01 UT
Location	Esrange Space Center, Sweden, 67.9°N			Wallops I., USA, 38°N	ECOMA campaigns, Andøya Rocket Range, Norway, 69.3°N					Esrange S. C., Sweden
Apogee	95.1 km			97.9 km	130.6 km		125.3 km	125.4 km	123.1 km	107.7 km
Grid 1	59.1 - 65.4 km	61.2 - 67.4 km	63.1 - 69.1 km	-	68.4 - 73.2 km	78.3 - 82.7 km	66.5 - 71 km	84.5 - 88.0 km	65.5 - 70 km	Ref., open
Grid 2	67.8 - 73.3 km	69.4 - 74.7 km	71.0 - 76.2 km	Ref.	78.1 - 86.2 km	85.5 - 89.6 km	76 - 88.5 km	Ref.	75 - 87 km	Ref., covered
Grid 3	75.2 - 79.8 km	76.5 - 81.0 km	77.8 - 82.1 km	70.3 - 74.5 km	88.9 - 92.7 km	92.2 – 96.0 km	91 - 95.5 km	92.5 - 102.5 km	90 - 94 km	Ref., open
Grid 4	81.3 - 84.9 km	82.4 - 85.9 km	83.5 - 86.8 km	76.7 - 93.5 km	95.2 - 98.8 km	98.3 - 101.8 km	98 - 102 km	104.5 - 107.5 km	96.5 - 100.5 km	77.3 - 91.0 km
Grid 5	86.3 - 89.3 km	87.1 - 89.9 km	87.9 - 90.6 km	94.5 - 97.0 km	101 - 104.3 km	104.0 - 107.1 km	Ref.	Ref.	Ref.	Ref., covered
Grid 6	90.3 - 92.4 km	90.8 - 92.8 km	91.4 - 93.2 km	Ref.	106.3 - 109.3 km	109.1 - 111.9 km	Ref.	111.0 - 113.5 km	Ref.	Ref., open
Grid 7	93.0 - 94.3 km	93.3 - 94.5 km	93.7 - 94.7 km	Ref.	111.0 - 115.8 km	113.6 - 116.1 km	-	-	-	Ref., open
Grid 8	Ref.	Ref.	Ref.	-	Ref.	Ref.	-	-	-	Ref., covered
Grid 9	Ref.	Ref.	-	-	Ref.	Ref.	-	-	-	-
HCC[1]	79-85 km			-	80-90 km		77-95 km	81-95 km	70-95 km	81-82 km
NLC	No, outside NLC season			No, outside NLC season and region	No, outside NLC season		Yes 82-83 km	Yes[2] 82-85 km	Yes 81-85 km	Yes 81-82 km
	Non-NLC conditions, too warm for ice particles to form						Confirmed presence of ice by the on board NLC photometers			
Grid type	30 nm continuous carbon film on 200 lines/inch copper mesh			Ultra-thin C on holey C & 400 lines/in. Cu mesh	30 nm continuous C on 200 lines/in. Cu mesh, plasma cleaned (etched)		30 nm continuous C film on 200 lines/in. Cu mesh, plasma cleaned (etched)			Ultra-thin C on holey C & 400 lines/in. Cu mesh
Com-ments	Hydrocarbon film and particle contamination. Low contrast due to thick C film.			Particle cont. (too many particles)	Thick hydrocarbon film and drops, and lots of stainless steel particle contamination		Agglom. particles, no new nm particles	Particle contamination, C film heavily damaged, probably during transport		No cont., no in-flight sampled particles of any size

[1] HCC = heavy charge carriers. Indicates if charged particles were detected by other instruments and in what altitude region.

[2] Presence of NLC but confirmed absence of PMSE.

Figure

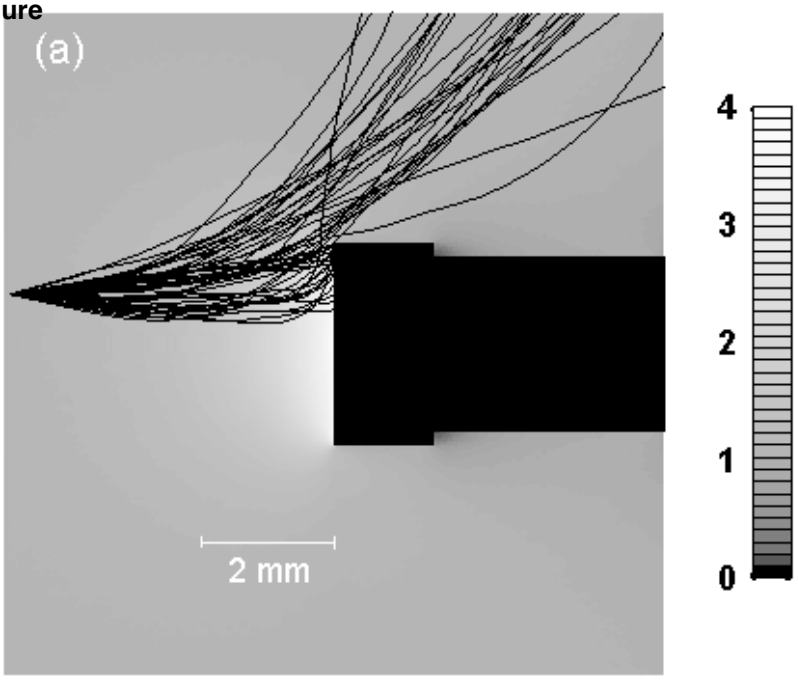

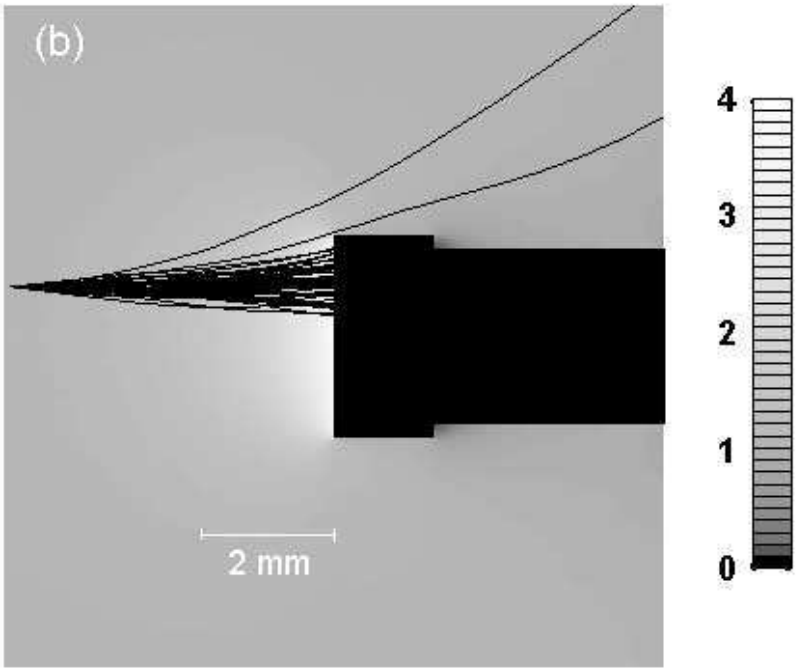

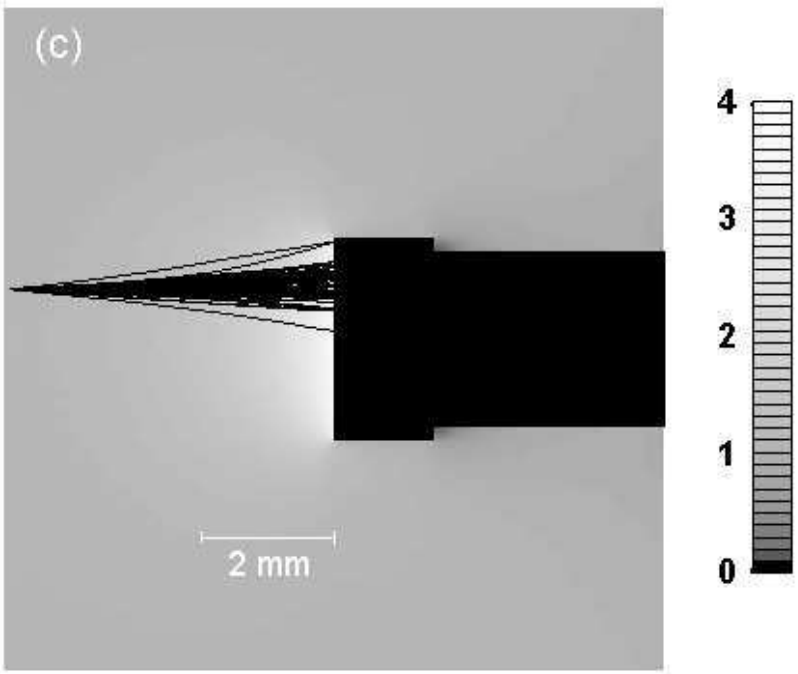

Figure

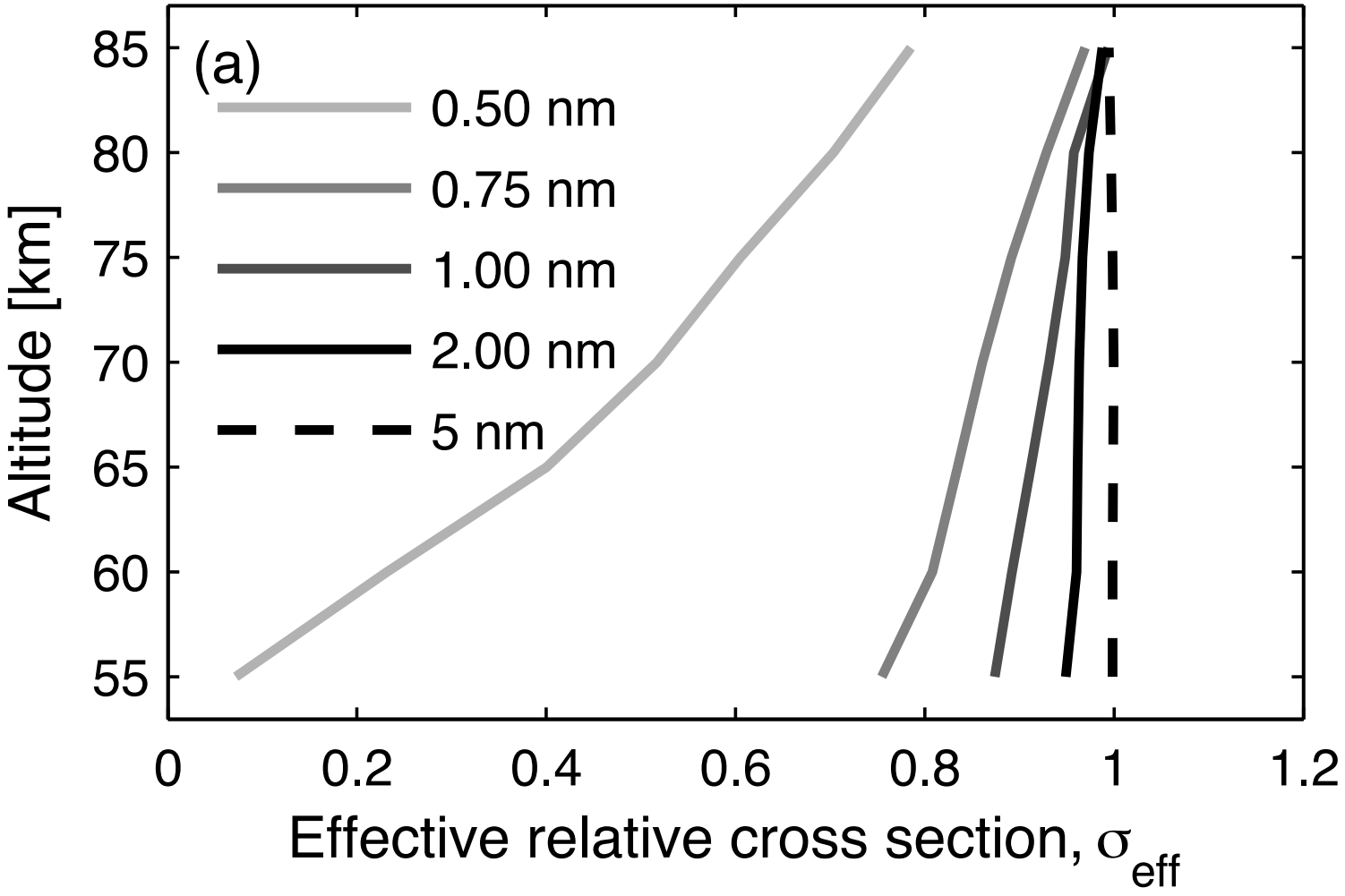
(a)
0.50 nm
0.75 nm
1.00 nm
2.00 nm
5 nm
Altitude [km]
85
80
75
70
65
60
55
0
0.2
0.4
0.6
0.8
1
1.2
Effective relative cross section, σeff

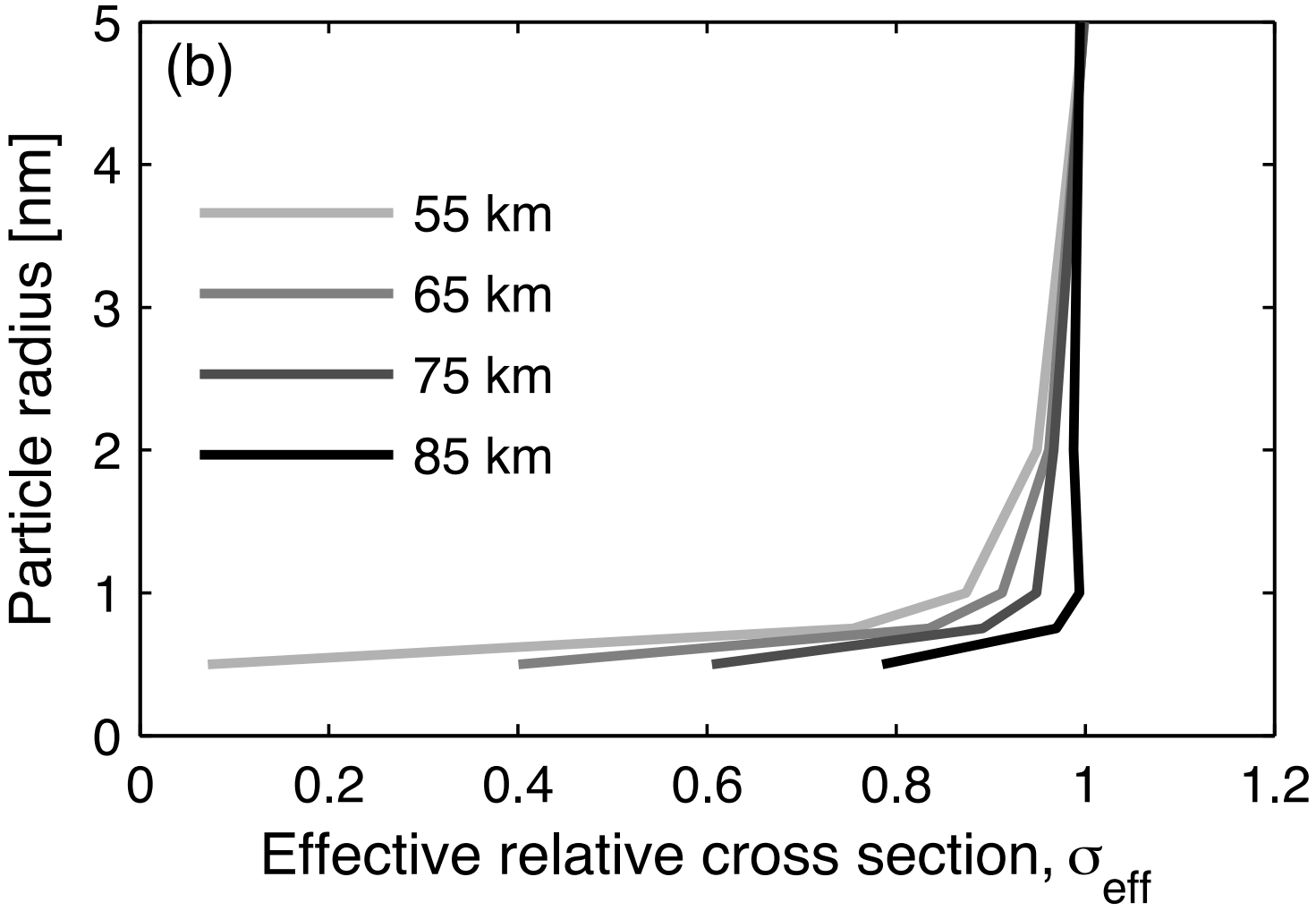
(b)
55 km
65 km
75 km
85 km
Particle radius [nm]
5
4
3
2
1
0
0
0.2
0.4
0.6
0.8
1
1.2
Effective relative cross section, σeff

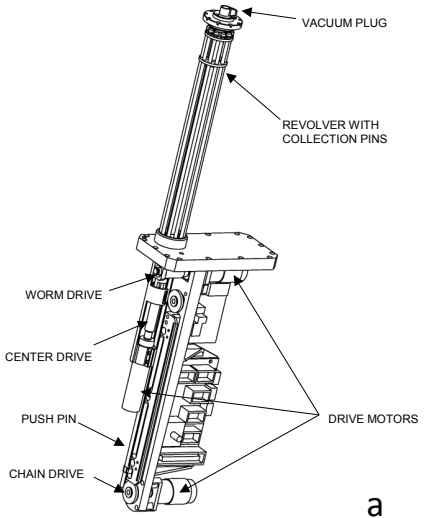
VACUUM PLUG
REVOLVER WITH
COLLECTION PINS
WORM DRIVE
CENTER DRIVE
PUSH PIN
CHAIN DRIVE
DRIVE MOTORS
a


b

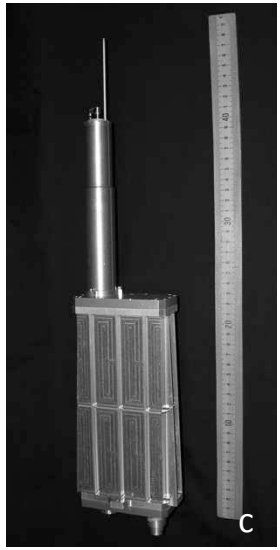
c


d

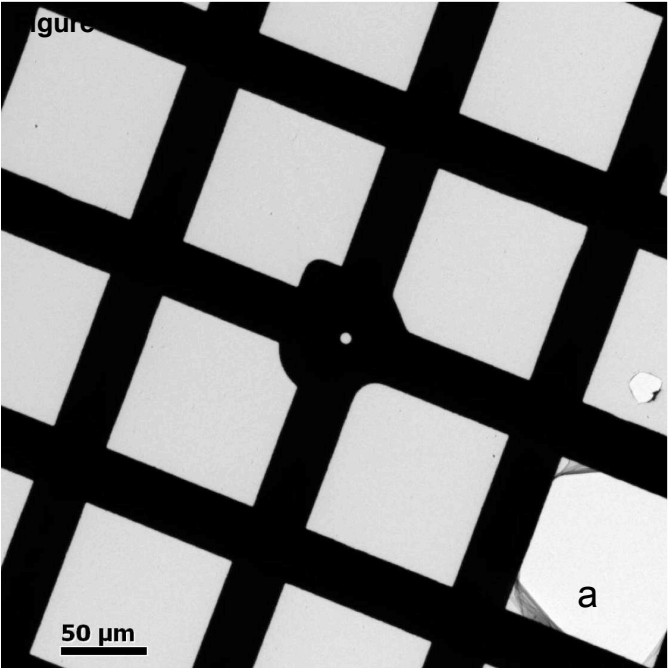
50 µm
a

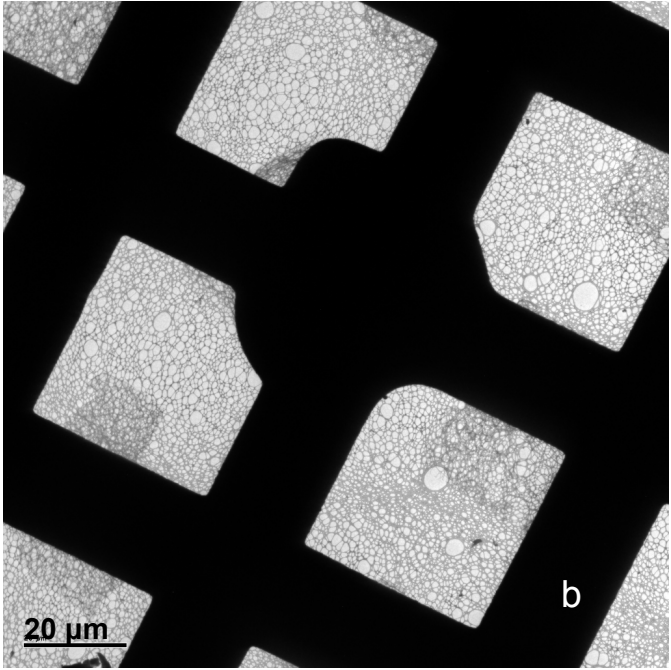
20 µm
b

Figure

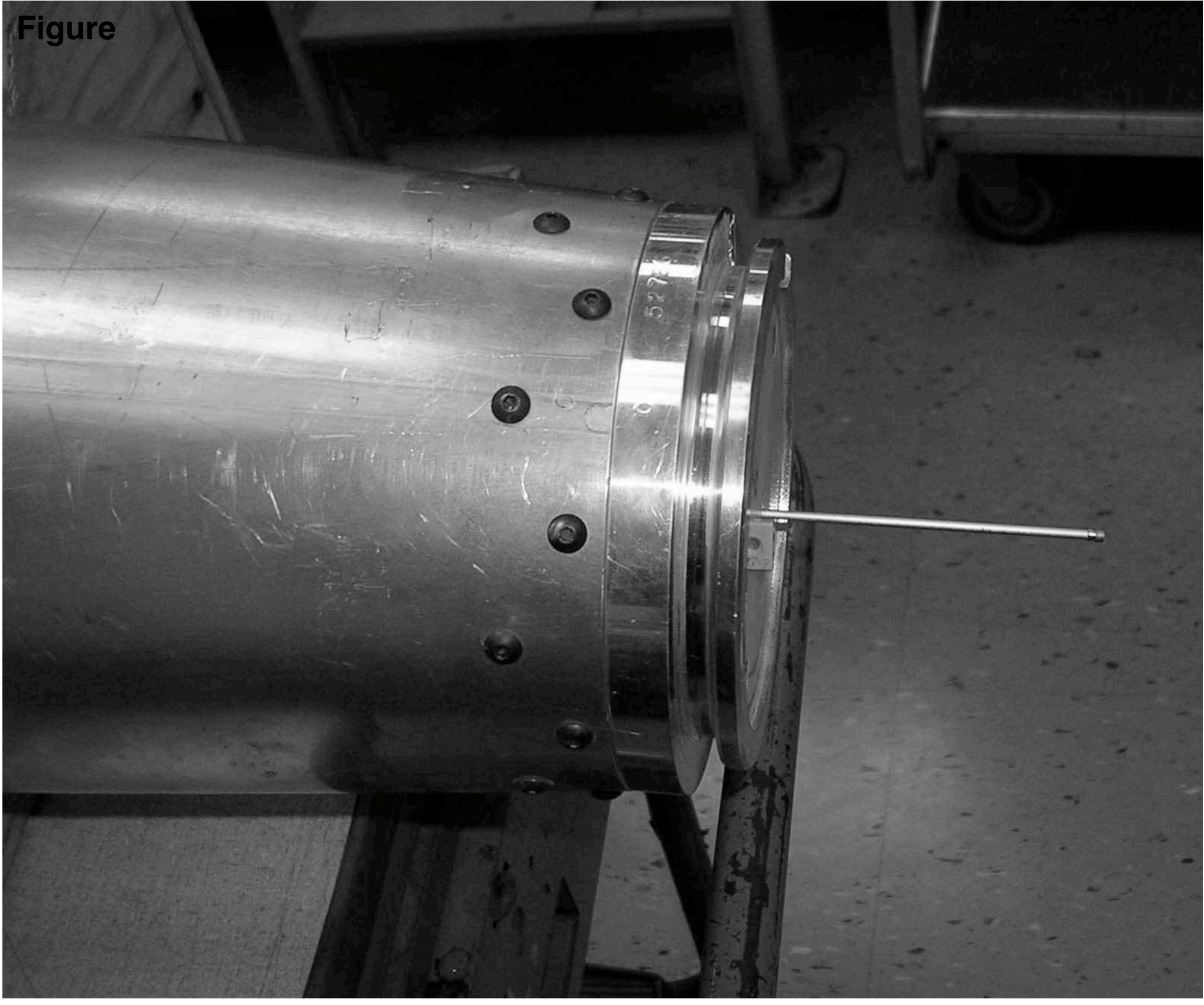

Figure

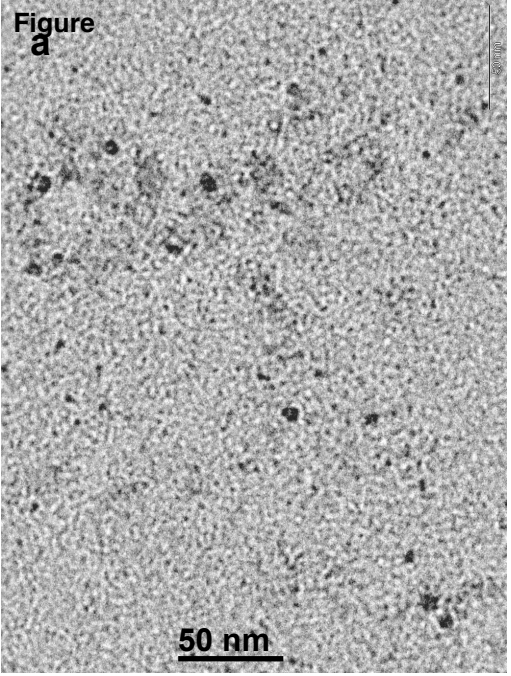

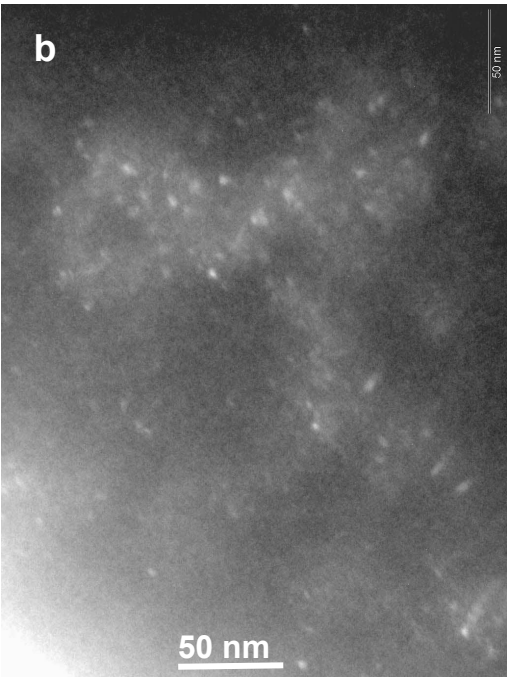

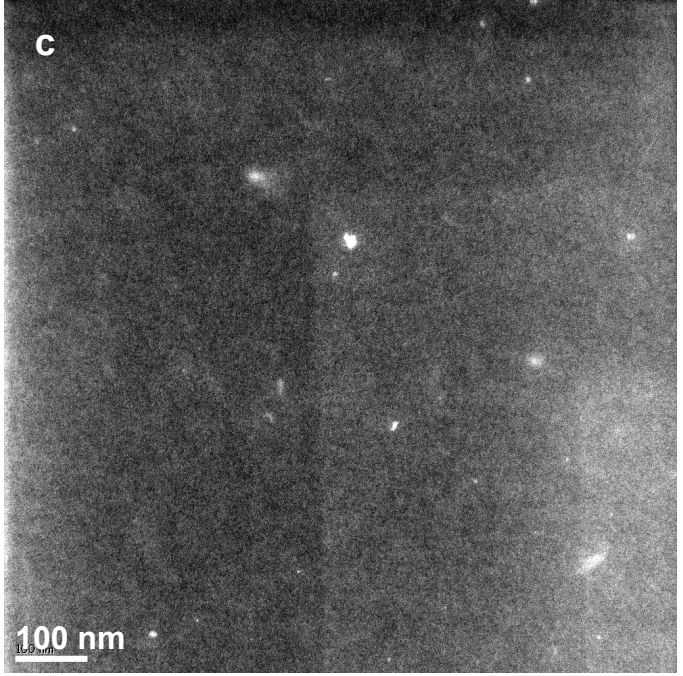

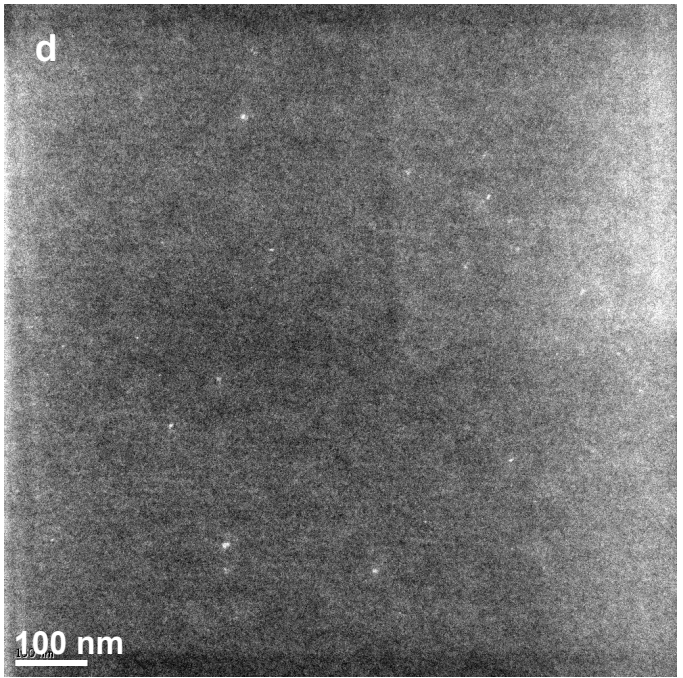

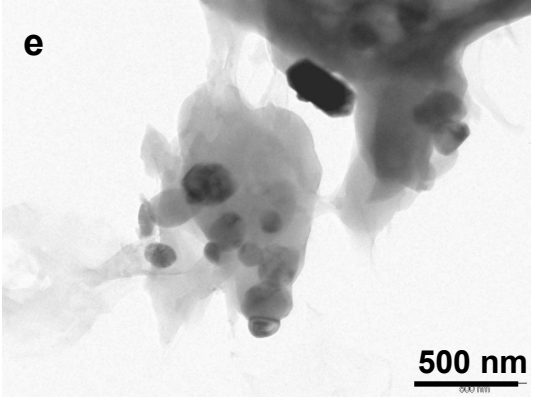

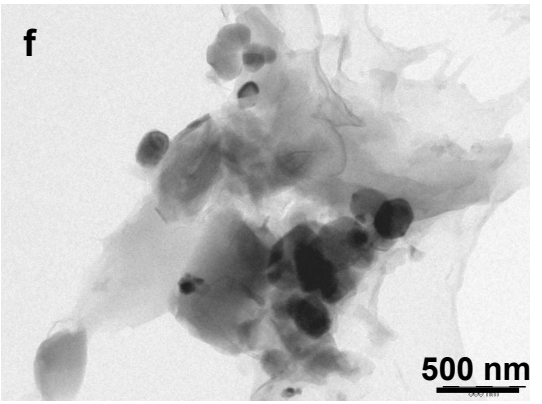

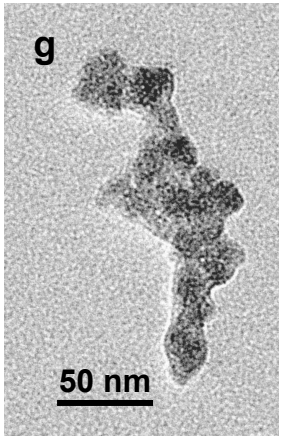

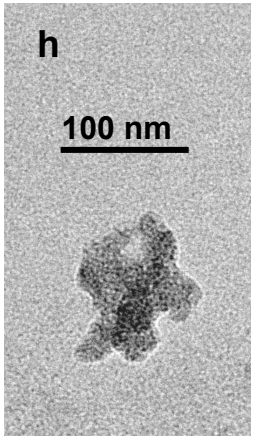

Figure

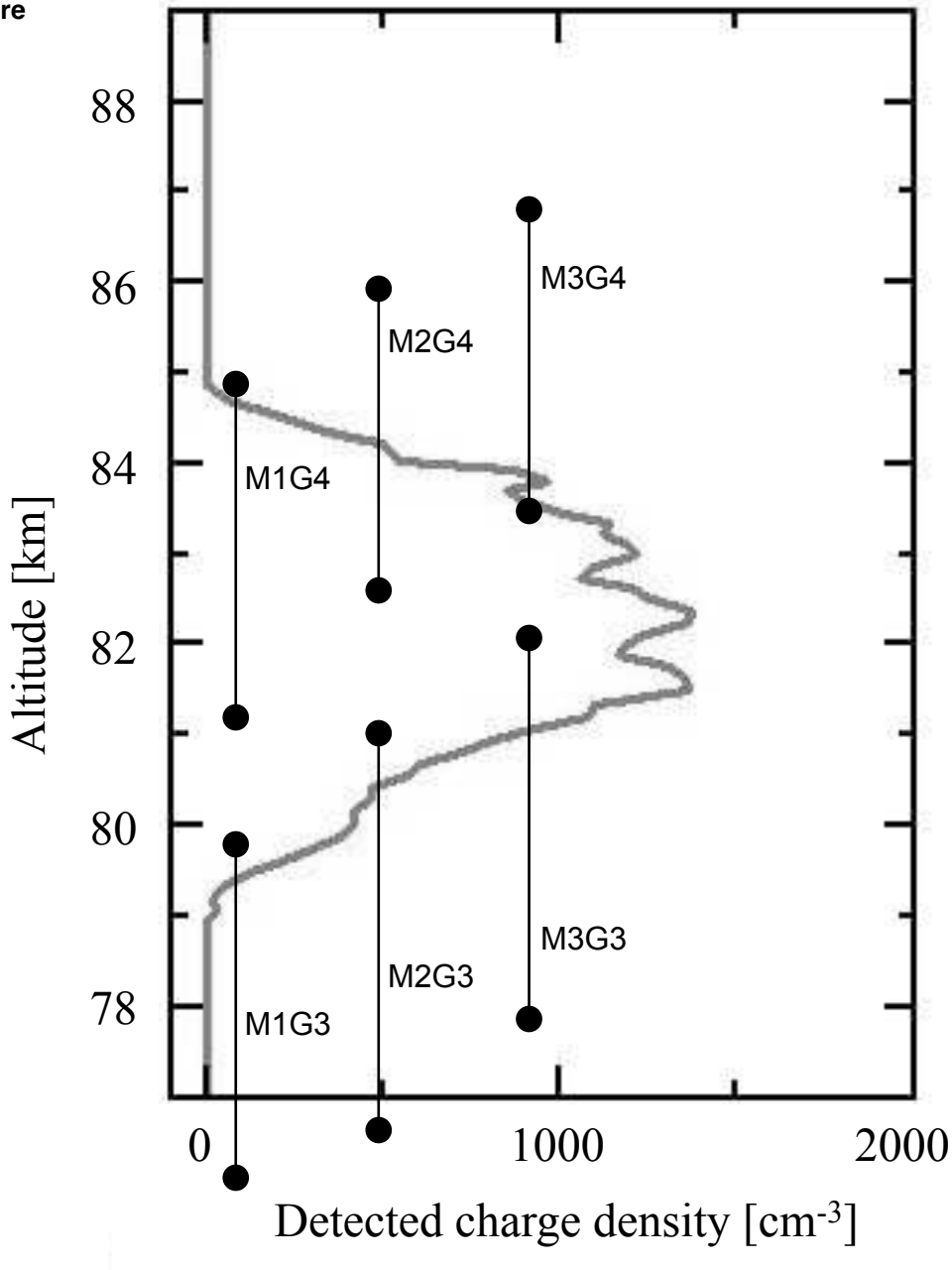
88
86
84
82
80
78
Altitude [km]
M3G4
M2G4
M1G4
M3G3
M2G3
M1G3
0
1000
2000
Detected charge density [cm-3]

Figure

Click here to download high resolution image

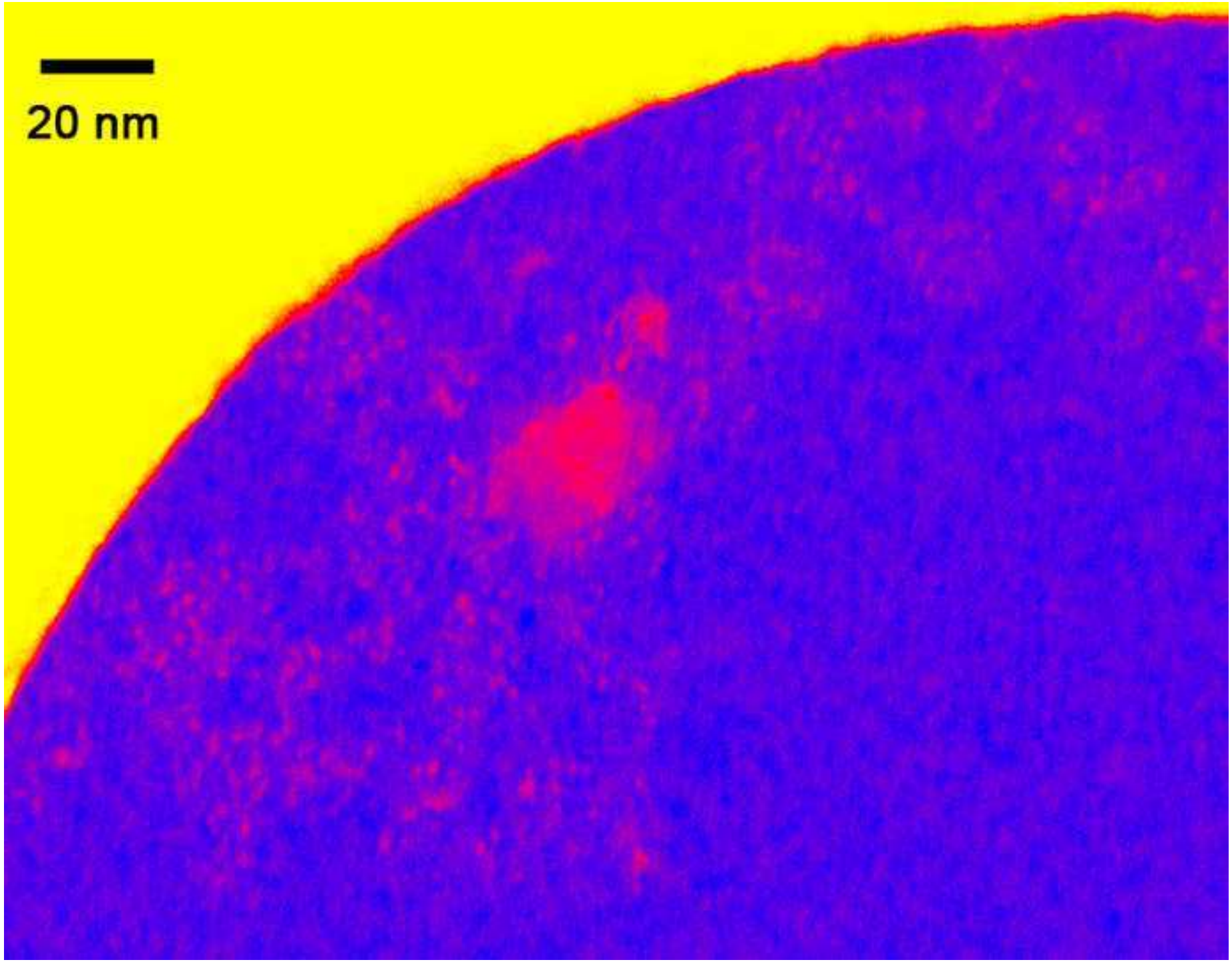

Figure

Click here to download high resolution image

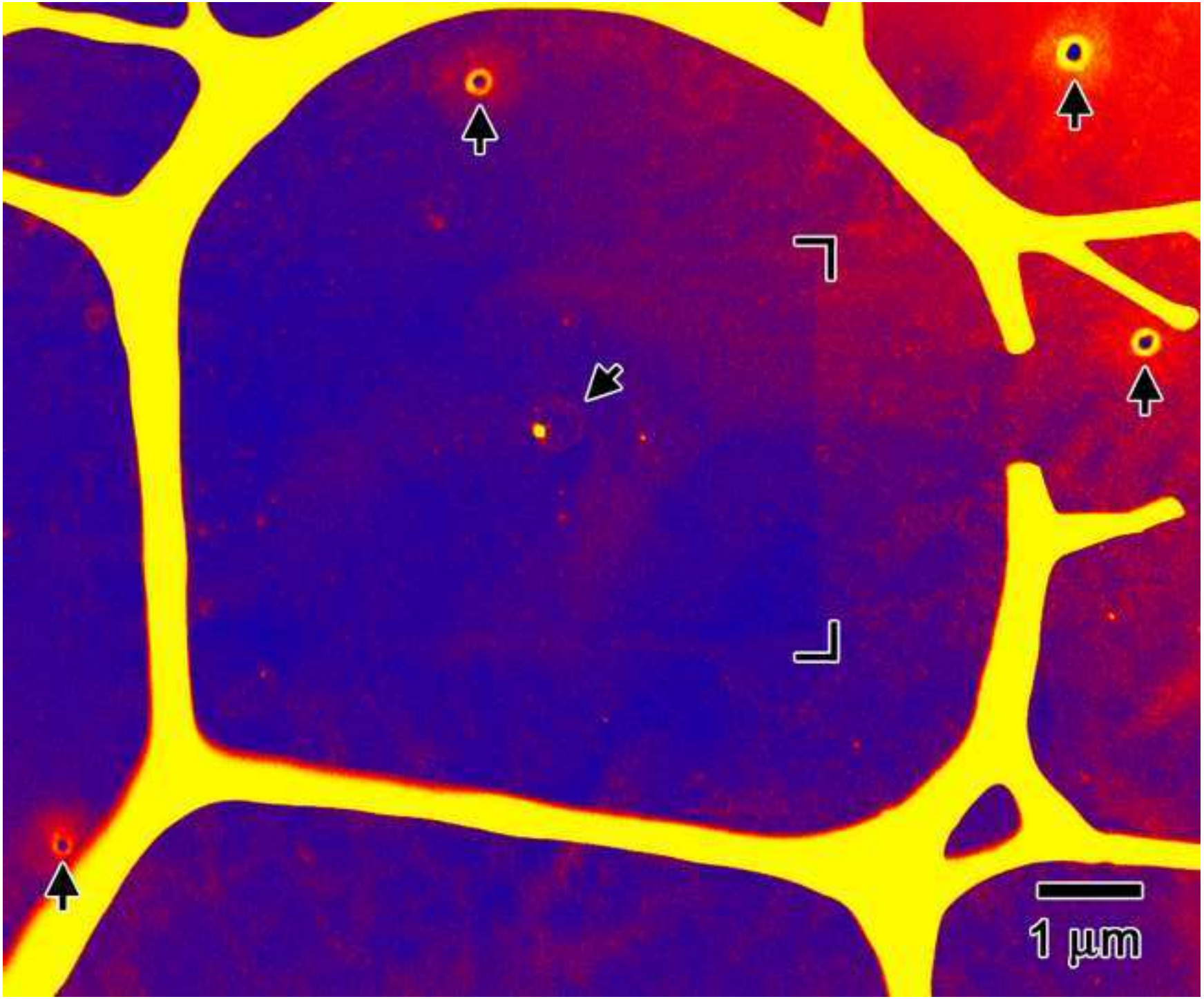

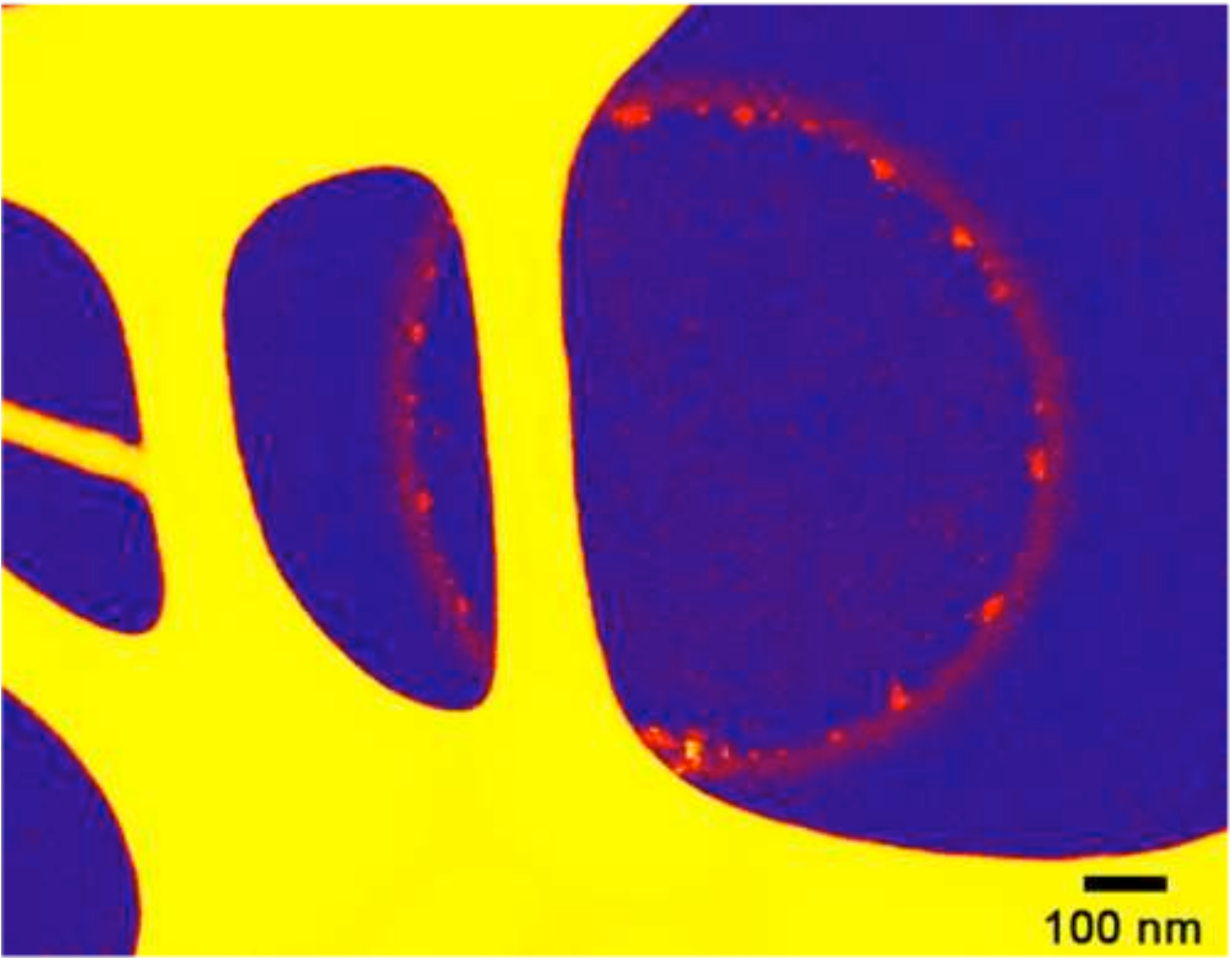
100 nm


a


b


c

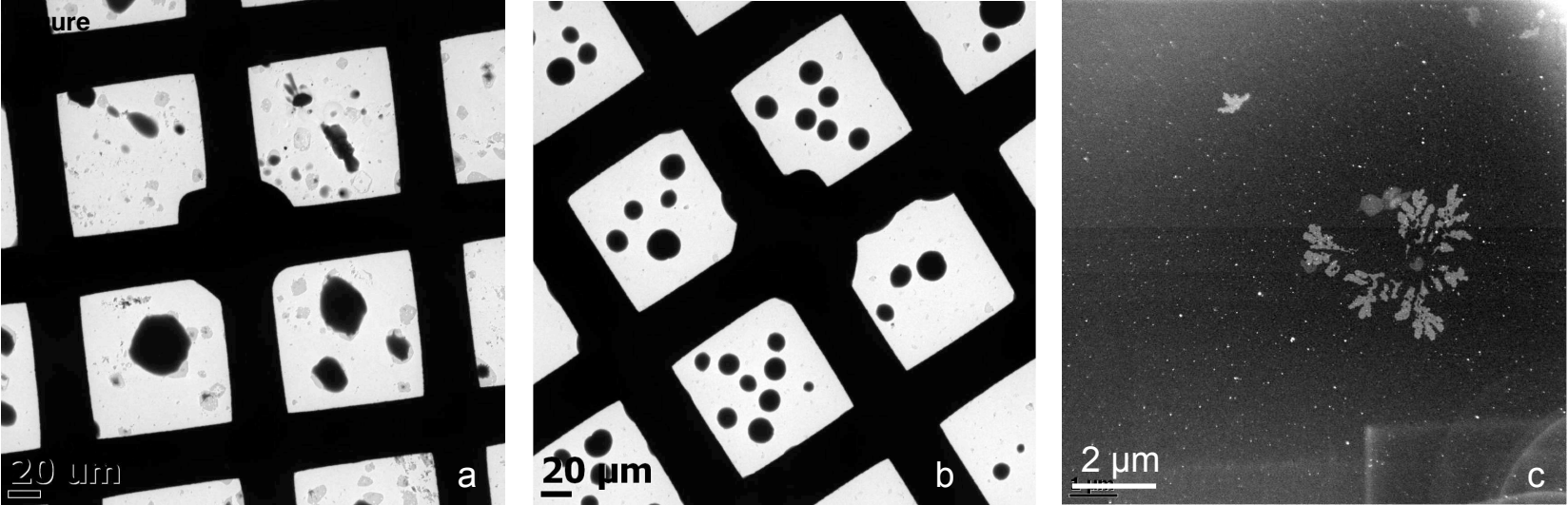
ure
20 um
a
20 µm
b
2 µm
c

Figure

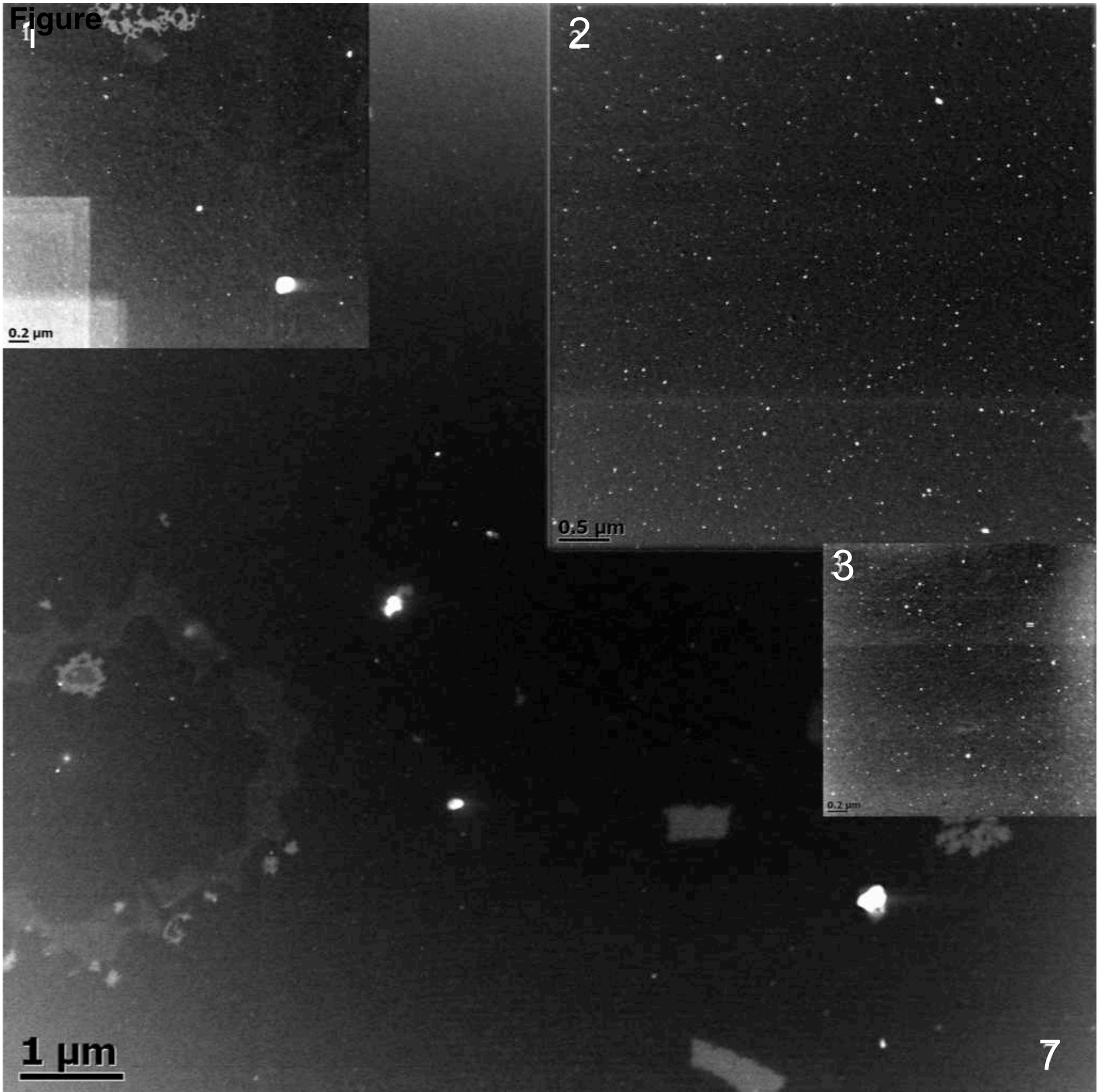

Figure

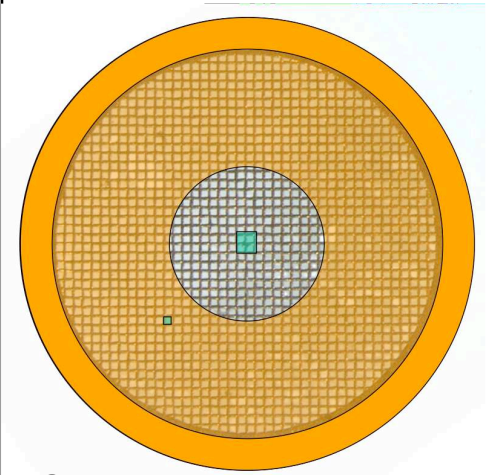
a

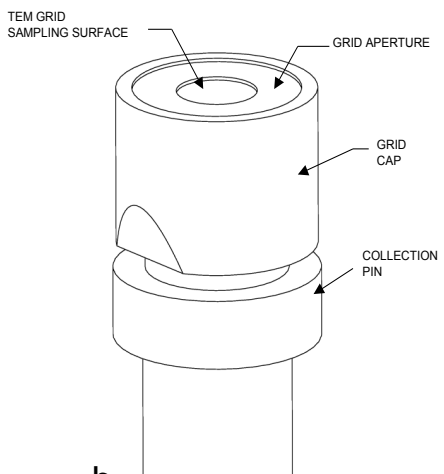
TEM GRID
SAMPLING SURFACE
GRID APERTURE
GRID
CAP
COLLECTION
PIN
b


c

Figure

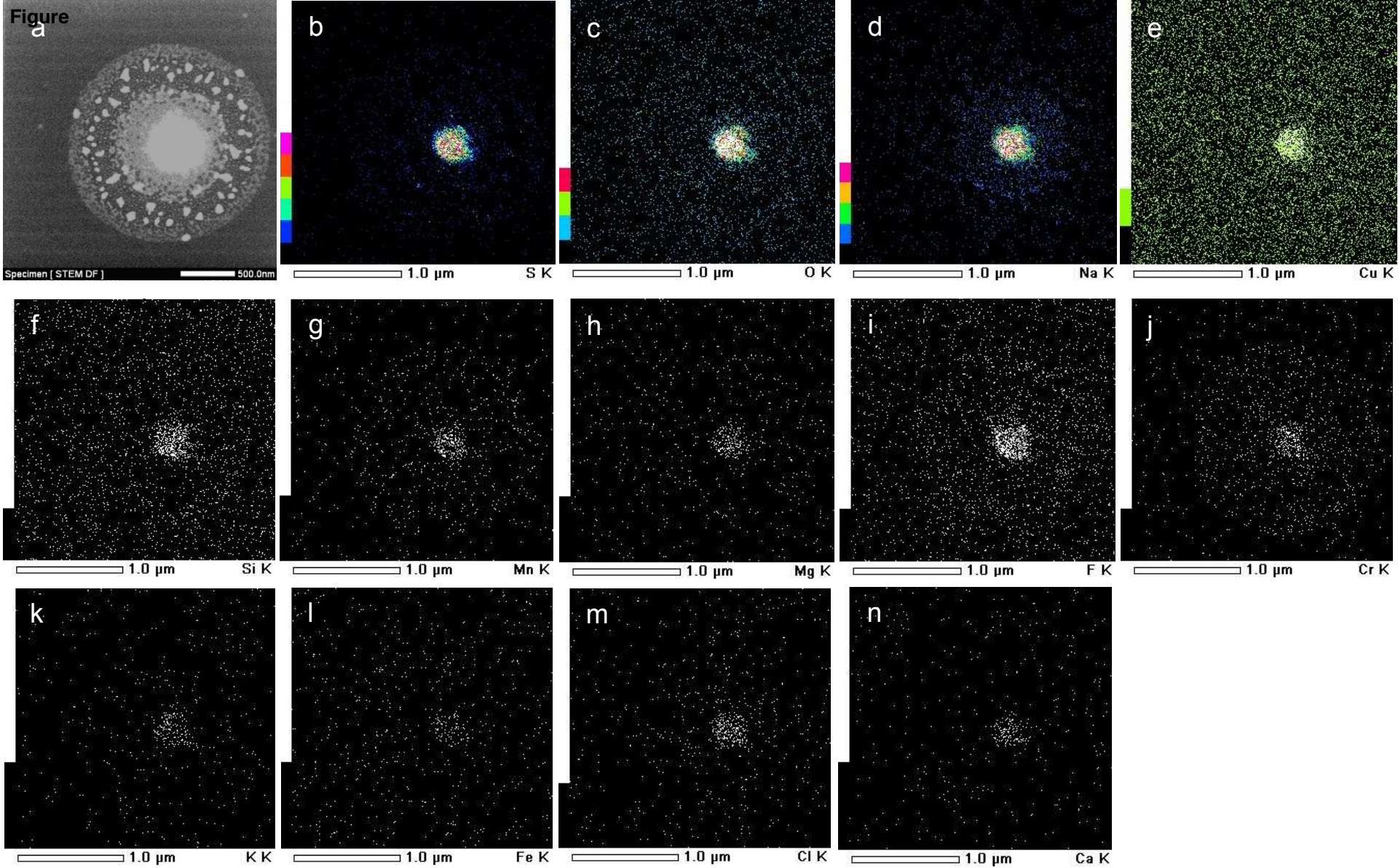
a
Specimen [STEM DF]
500.0nm
b
1.0 µm
S K
c
1.0 µm
O K
d
1.0 µm
Na K
e
1.0 µm
Cu K
f
1.0 µm
Si K
g
1.0 µm
Mn K
h
1.0 µm
Mg K
i
1.0 µm
F K
j
1.0 µm
Cr K
k
1.0 µm
K K
l
1.0 µm
Fe K
m
1.0 µm
Cl K
n
1.0 µm
Ca K

Figure

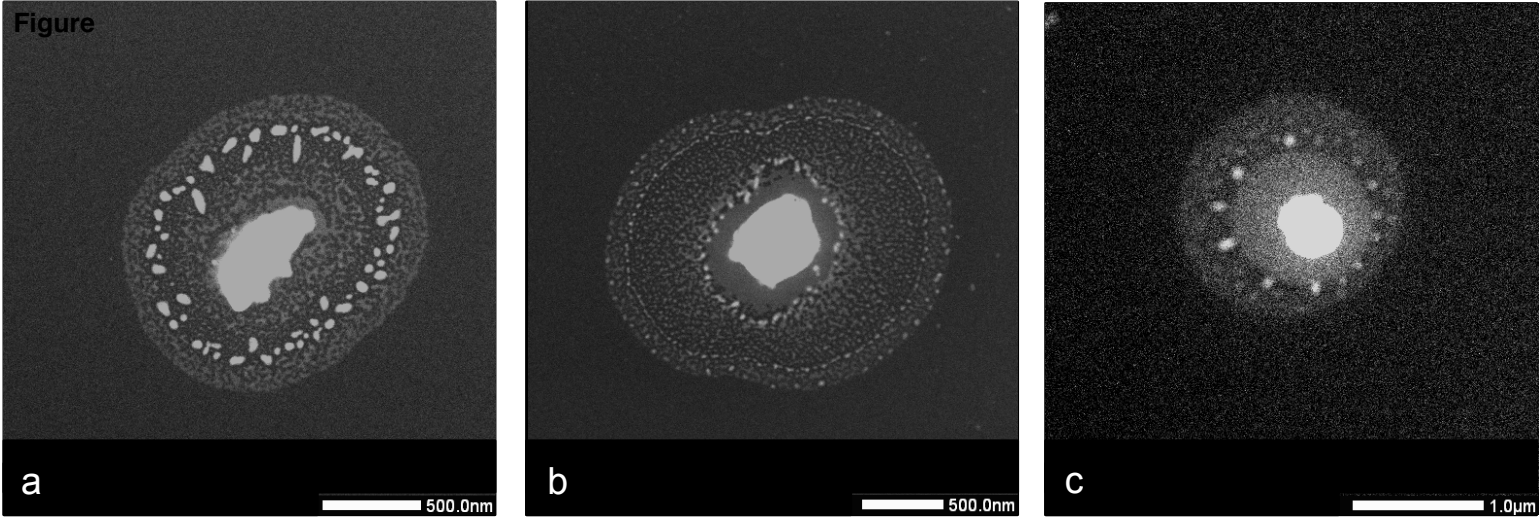


MAGIC

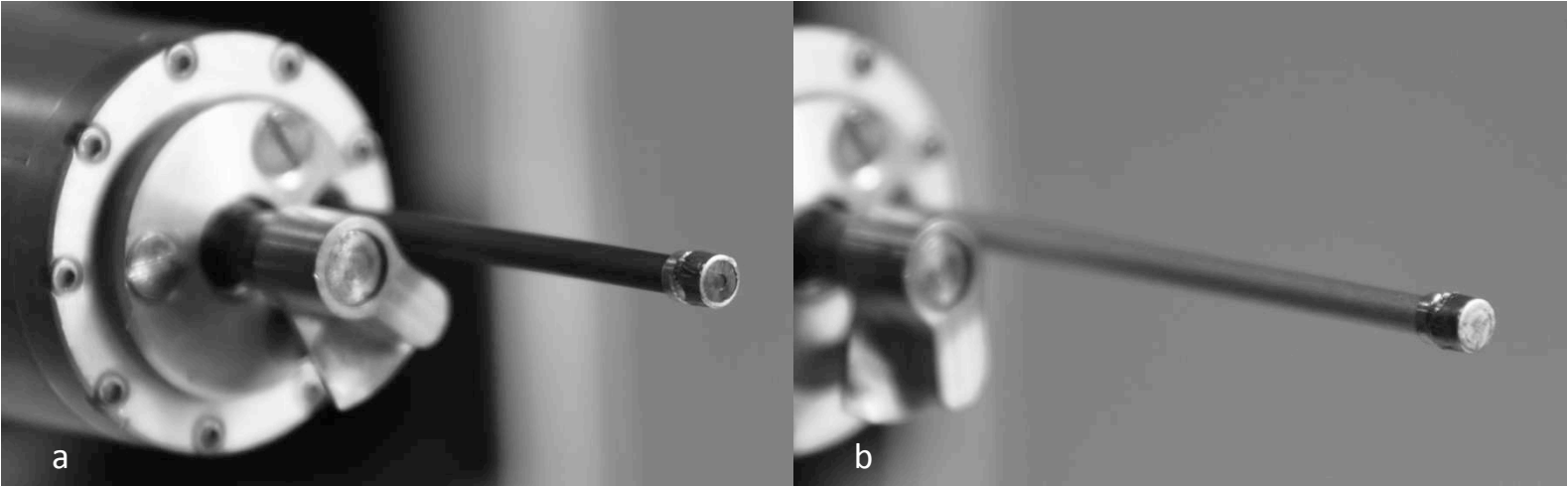
a
b